Article
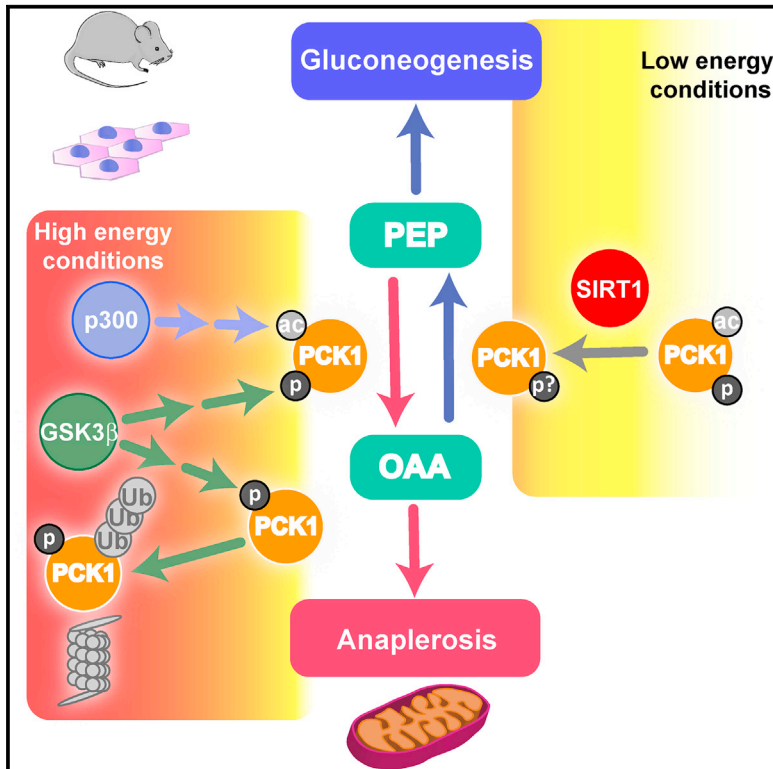
# Dynamic Acetylation of Phosphoenolpyruvate Carboxykinase Toggles Enzyme Activity between Gluconeogenic and Anaplerotic Reactions

## Graphical Abstract

## Authors

Pedro Latorre-Muro, Josue Baeza,
Eric A. Armstrong, ...,
Pascual López-Buesa,
José A. Carrodeguas, John M. Denu

## Correspondence

carrode@unizar.es (J.A.C.),
john.denu@wisc.edu (J.M.D.)

## In Brief

Latorre-Muro et al. report the regulation of PCK1 activity by post-translational modifications. p300-mediated acetylation drives PCK1 anaplerotic activity, whereas SIRT1 deacetylates and restores gluconeogenic activity. GSK3β-mediated phosphorylation leads to PCK1 ubiquitination and degradation. The interplay between acetylation, phosphorylation, and ubiquitination regulates PCK1 activity and stability and controls central metabolism.

## Highlights

- At high glucose, p300 hyperacetylates PCK1 and promotes anaplerosis

- At low glucose, SIRT1 deacetylates PCK1 and promotes gluconeogenesis

- GSK3β mediates PCK1 phosphorylation and promotes PCK1 degradation

- Crosstalk between acetylation, phosphorylation, and ubiquitination controls PCK1

CellPress

# Dynamic Acetylation of Phosphoenolpyruvate Carboxykinase Toggles Enzyme Activity between Gluconeogenic and Anaplerotic Reactions

Pedro Latorre-Muro,[1,2] Josue Baeza,[3] Eric A. Armstrong,[3] Ramón Hurtado-Guerrero,[2,4] Francisco Corzana,[5] Lindsay E. Wu,[6] David A. Sinclair,[6,7] Pascual López-Buesa,[1,2] José A. Carrodeguas,[2,8,9,*] and John M. Denu[3,10,11,*]

[1]Departamento de Producción Animal y Ciencia de los Alimentos, Facultad de Veterinaria, Universidad de Zaragoza, 50013 Zaragoza, Spain
[2]Instituto de Biocomputación y Física de Sistemas Complejos (BIFI), BIFIIQFR (CSIC) Joint Unit, Universidad de Zaragoza, 50018 Zaragoza, Spain
[3]Wisconsin Institute for Discovery and Department of Biomolecular Chemistry, University of Wisconsin School of Medicine and Public Health–Madison, Madison, WI 53715, USA
[4]Fundación ARAID, Government of Aragón, Zaragoza, Spain
[5]Departamento de Química, Centro de Investigación en Síntesis Química, Universidad de La Rioja, 26006 Logroño, Spain
[6]Department of Pharmacology, School of Medical Sciences, The University of New South Wales, Sydney, NSW 2052, Australia
[7]Department of Genetics, Paul F. Glenn Laboratories for the Biological Mechanisms of Aging, Harvard Medical School, Boston, MA 02115, USA
[8]Departamento de Bioquímica y Biología Molecular y Celular, Facultad de Ciencias, Universidad de Zaragoza, 50009 Zaragoza, Spain
[9]IIS Aragón, Zaragoza, Spain
[10]Morgridge Institute for Research, Madison, WI 53715, USA
[11]Lead Contact
*Correspondence: carrode@unizar.es (J.A.C.), john.denu@wisc.edu (J.M.D.)
https://doi.org/10.1016/j.molcel.2018.07.031

## SUMMARY

Cytosolic phosphoenolpyruvate carboxykinase (PCK1) is considered a gluconeogenic enzyme; however, its metabolic functions and regulatory mechanisms beyond gluconeogenesis are poorly understood. Here, we describe that dynamic acetylation of PCK1 interconverts the enzyme between gluconeogenic and anaplerotic activities. Under high glucose, p300-dependent hyperacetylation of PCK1 did not lead to protein degradation but instead increased the ability of PCK1 to perform the anaplerotic reaction, converting phosphoenolpyruvate to oxaloacetate. Lys91 acetylation destabilizes the active site of PCK1 and favors the reverse reaction. At low energy input, we demonstrate that SIRT1 deacetylates PCK1 and fully restores the gluconeogenic ability of PCK1. Additionally, we found that GSK3β-mediated phosphorylation of PCK1 decreases acetylation and increases ubiquitination. Biochemical evidence suggests that serine phosphorylation adjacent to Lys91 stimulates SIRT1-dependent deacetylation of PCK1. This work reveals an unexpected capacity of hyperacetylated PCK1 to promote anaplerotic activity, and the intersection of post-translational control of PCK1 involving acetylation, phosphorylation, and ubiquitination.

## INTRODUCTION

Cytosolic phosphoenolpyruvate carboxykinase (PCK1) is a major regulator of gluconeogenesis, glyceroneogenesis, and cataplerosis in the tricarboxylic acid (TCA) cycle (Yang et al., 2009a). PCK1 regulates an essential rate-limiting step by catalyzing the reversible conversion of oxaloacetate (OAA) into phosphoenolpyruvate (PEP). Through tissue-specific transcription factors, PCK1 transcription is regulated by various stimuli (Hanson and Reshef, 1997). Outside gluconeogenesis, the metabolic functions of PCK1 are not well understood. The ability to catalyze a reversible reaction, and thus synthesize OAA from PEP, indicates that PCK1 could also have a role in anaplerosis, replenishing the TCA cycle (Hakimi et al., 2007). Yet the conditions by which PCK1 triggers the synthesis of OAA in the cell are not known. Mice lacking PCK1 in the liver showed alterations in gene expression and lipid metabolism (She et al., 2000) but displayed only a slight decrease in glucose synthesis (She et al., 2003). Burgess et al. (2007) reported that murine liver lacking PCK1 had only a 43% reduction in total glucose production and suggest a role of PCK1 in the TCA cycle, integrating energy metabolism. Together, these observations suggest a more complex metabolic role for PCK1 and one that might require a more rapid regulatory mechanism in response to energy input.

There is evidence that PCK1 is acetylated in yeast (Lin et al., 2009) and in cultured human cells (Zhao et al., 2010); however, the function of acetylation is unclear. In yeast, acetylation was suggested to stimulate Pck1p activity (Lin et al., 2009), while acetylation in cultured mammalian cells was reported to induce
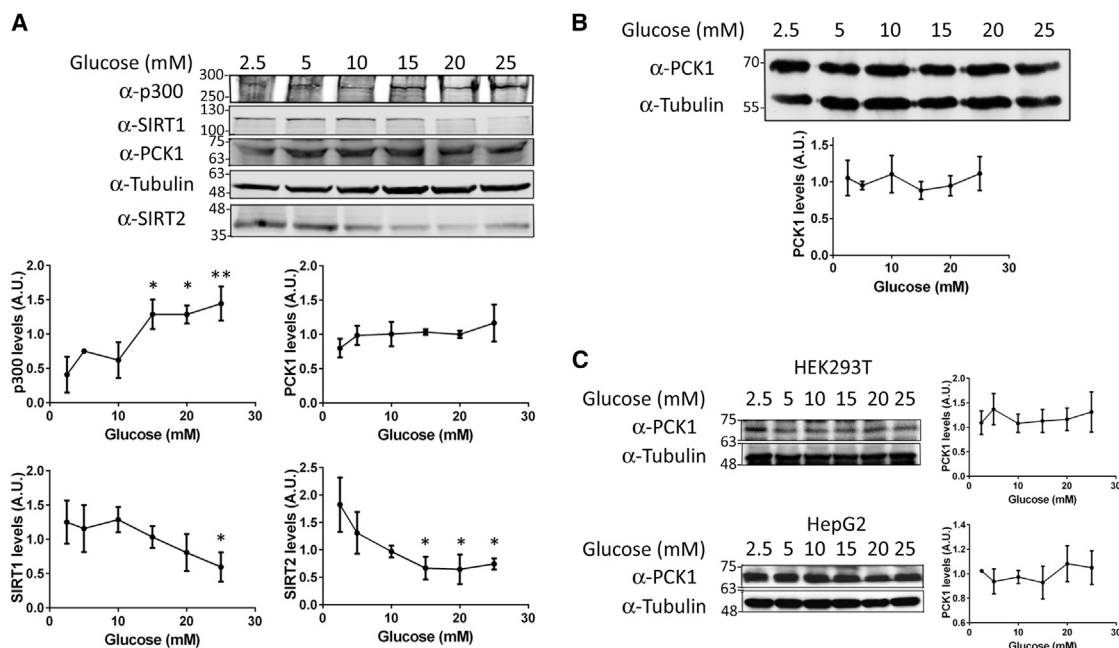
**Figure 1. PCK1 Protein Levels Are Not Altered by Glucose Concentration**
(A) PCK1 protein levels remained constant over a wide range of glucose concentrations. HEK293T cells were exposed to different glucose concentrations, n = 3.
(B) Endogenous PCK1 protein levels in HepG2 cells display no significant change over a wide range of glucose concentrations (n = 4).
(C) Same experiment as (A) and (B) in HEK293T and HepG2 cells but using media containing FBS (n = 2).
In (A)–(C), numbers on the left indicate molecular weight (kDa). Mean ± SD are represented. Significances are referred to the 2.5 mM condition, *p < 0.05, ** p < 0.01.

the degradation of PCK1 protein (Jiang et al., 2011). Proteomic analyses have reported phosphorylation on PCK1 in different species (Bian et al., 2014; Grimsrud et al., 2012; Wilson-Grady et al., 2013), but no functional consequence was reported.

Here, we investigated how mammalian PCK1 is regulated at the post-translational level in response to varying energy inputs. PCK1 acetylation is regulated by p300 acetyltransferase under high glucose and, conversely, SIRT1 deacetylates PCK1 under low-energy conditions. The enzymatic properties of recombinant, site-specifically acetylated enzyme, and of PCK1 purified from cultured cells and from wild-type and SIRT1 knockout murine tissues reveal a novel mechanism: acetylation under high glucose concentrations triggers PCK1 anaplerotic activity and SIRT1-mediated deacetylation promotes the gluconeogenic activity. Also, we discovered that PCK1 phosphorylation is mediated by the GSK3β pathway and controls PCK1 stability in cells by increasing PCK1 ubiquitination and degradation. Additionally, our results suggest that phosphorylation affects the efficiency by which SIRT1 deacetylates PCK1. Together, these results reveal a previously unknown intersection of post-translational control of PCK1 involving acetylation, phosphorylation, and ubiquitination that regulates central metabolism.

## RESULTS

### Cells Maintain a Constant Pool of PCK1 under a Wide Range of Glucose Concentrations

PCK1 is widely considered a gluconeogenic enzyme (Yang et al., 2009a) and under high glucose is thought to serve no significant function (Jiang et al., 2011). *PCK1* mRNA half-life is relatively short (30 min) (Granner et al., 1983; Hod and Hanson, 1988; Tilghman et al., 1974) and its RNA transcription is repressed under high-glucose conditions (Shao et al., 2005) by insulin (Yang et al., 2009b). However, other studies have implicated additional roles in metabolism (Burgess et al., 2007; She et al., 2000, 2003), belying its lack of function in these replete conditions. In rat tissues, the PCK1 protein half-life is relatively long, up to 20 hr during starvation and 6–8 hr during re-feeding (Hopgood et al., 1973), and in some cases no degradation was observed (Philippidis et al., 1972). Others have suggested that protein acetylation regulates PCK1 stability (Jiang et al., 2011). To investigate these apparent discrepancies, we set up a series of experiments to study the role of acetylation in modulating PCK1 function and to investigate the potential functions of PCK1 during energy-replete conditions. First, we quantified the glucose-regulated levels of endogenous PCK1, protein acetyltransferase p300, and SIRT1 and SIRT2 deacetylases, which have been implicated in PCK1 acetylation (Jiang et al., 2011; Lin et al., 2009). After 24 hr of HEK293T cells' exposure to different glucose concentrations, PCK1 levels remained invariable, whereas SIRT1 and SIRT2 protein levels decreased, and the acetyltransferase p300 increased at higher glucose concentrations (Figure 1A). Similarly, varied glucose levels had no significant effects on PCK1 protein levels in HepG2 cells (Figure 1B). The steady-state levels of PCK1 were also insensitive to the presence (Figure 1C) or absence (Figures 1A and 1B) of 10% fetal bovine serum (FBS) when glucose was varied. These results using two human gluconeogenic cell lines indicated that steady-state levels of PCK1 are
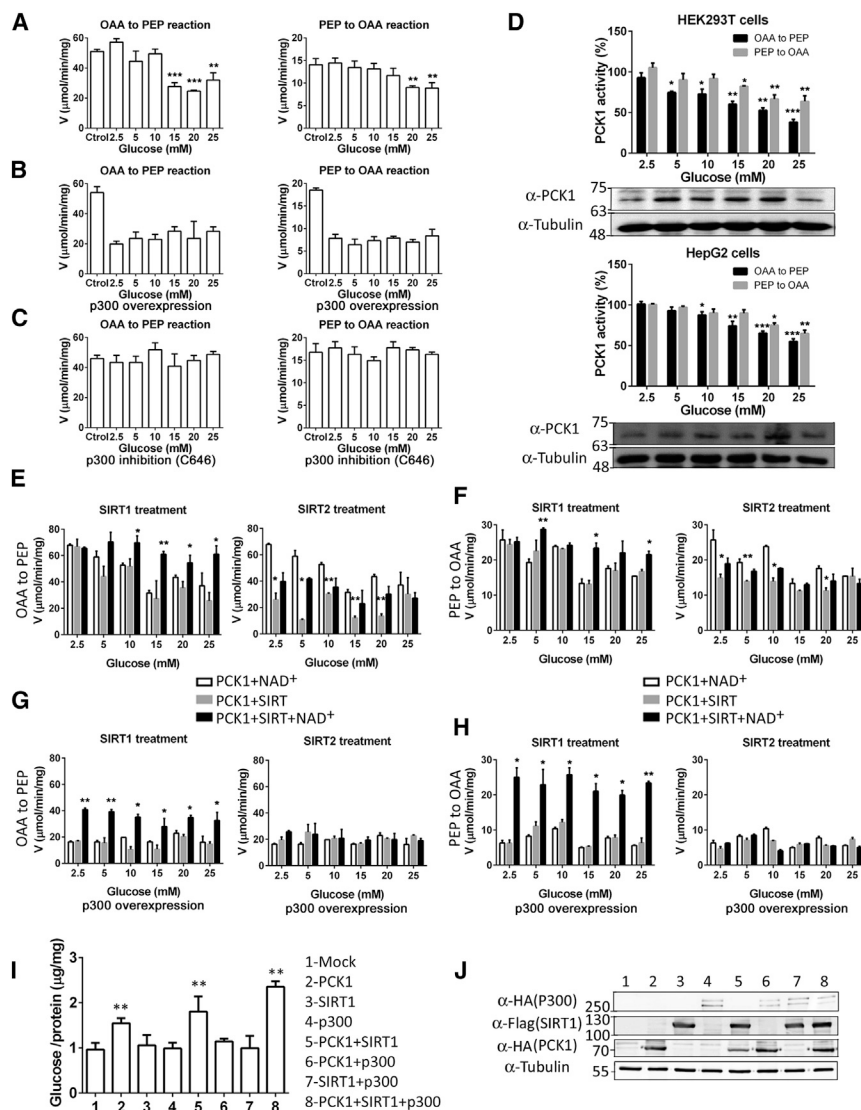
**Figure 2. P300-Mediated Acetylation Modifies PCK1 Activity**

(A) Glucose concentration affects PCK1 activity in cells. Activity of PCK1 purified from HEK293T cells exposed to different glucose concentrations was measured in both reaction directions. Recombinant PCK1 purified from *E. coli* was used as control (see also Figure S1A).

(B) The experiment described in (A) was repeated, but with co-transfection of PCK1 and human p300 (see also Figures S1A and S1B).

(C) The experiment described in (A) was repeated, but with inhibition of p300 using C646 at 10 μM for 24 hr.

(D) Endogenous PCK1 activity is modified by the presence of glucose in cell media. PCK1 activity was measured in both reaction directions using cytosolic fractions from HEK293T and HepG2 cells (n = 3).

(E–H) SIRT1 recovers PCK1 activity in both reaction directions. PCK1 activity obtained from experiment (A) was measured in (E) OAA→PEP and (F) PEP→OAA reaction directions after recombinant SIRT1 or SIRT2 treatment. (G) and (H) are the same experiment as (E) and (F), but using protein from experiment (B).

(I) Acetylation modifies PCK1 gluconeogenic activity. Glucose production was determined in HEK293T cells overexpressing different combinations of PCK1, SIRT1, and p300. Graph represents glucose production after 6 hr of incubation. Mean ± SD are represented, n = 3, **p < 0.01 (see Figure S1C).

(J) Overexpression of different proteins during glucose assays described in (I). Numbers on the left indicate molecular weight (kDa).

In (A)–(H), mean ± SD are represented. PCK1 activity for each condition was compared to that of PCK1 purified from the 2.5-mM condition. *p < 0.05, **p < 0.01, ***p < 0.001, n = 3 in (A)–(D) and n = 2 in (E)–(H). Only those values referred in the main text are represented.

stable across a wide range of glucose concentrations, while enzymes that control protein acetylation (p300, SIRT1, and SIRT2) displayed altered levels. Together, these results suggest that PCK1 activity might be regulated by acetylation.

## PCK1 Activity Is Glucose Dependent and Regulated by p300 and SIRT1

We explored the possibility that in response to high glucose, p300 acetylates PCK1 and alters its catalytic activity. Due to the broad kinetic and structural information of rat PCK1 (Cui et al., 2017; Johnson and Holyoak, 2010, 2012; Johnson et al., 2016), the rat enzyme was overexpressed and purified as a His-tagged protein from HEK293T cells exposed to different glucose concentrations (Figure S1A). PCK1 activity was measured under $V_{max}$ conditions (saturating levels of substrates) in both forward and reverse reaction directions and compared to the identical recombinant protein expressed and purified from *E. coli*, as a control. Glucose above 10 mM decreased PCK1

activity down to 45% of control in the gluconeogenic direction (OAA→PEP), whereas a slight (20%) reduction was observed in the reverse direction (PEP→OAA) (Figure 2A). Recombinant PCK1 purified from *E. coli* displayed the same specific activity as PCK1 purified from HEK293T cells exposed to low glucose. These observations suggest that high glucose leads to a modified form of PCK1 that displays reduced activity in the gluconeogenic direction.

To examine the possibility that PCK1 is hyperacetylated under high glucose and rendered less active in the gluconeogenic direction, we co-transfected HEK293T cells with rat PCK1 and human p300 and assessed PCK1 activity at varied glucose. Under conditions of PCK1 and p300 combined expression, PCK1 activity dropped to 40% of control in both reaction directions and was no longer dependent on glucose concentration (Figure 2B). Additionally, the glucose-dependent effect on PCK1 activity was not observed when p300 was inhibited using C646 (Figure 2C), suggesting that p300 mediated the loss of

PCK1 activity. In a separate experiment, PCK1 was not a direct substrate of acetyltransferase TIP60 (Figure S1B) (Lin et al., 2009; Xiao et al., 2014).

To determine the effects of varied glucose levels on endogenous PCK1 protein, cytosolic fractions from HEK293T and HepG2 cells were isolated and endogenous PCK1 activity was measured in both reaction directions under $V_{max}$ conditions. At high glucose concentrations, PCK1 gluconeogenic activity decreased (down to 33% and 55% of control activity in HEK293T and HepG2 cells, respectively), whereas the PEP→OAA activity was maintained at ≥70% in both cell lines) (Figure 2D).

To investigate whether reversible acetylation was responsible for the observed differences in activity, PCK1 purified from HEK293T cells was incubated with either recombinant SIRT1 or SIRT2 deacetylases purified from *E. coli*, and $V_{max}$ activity of PCK1 was measured. Only SIRT1 recovered PCK1 activity in the forward (OAA→PEP) (Figure 2E) and reverse (PEP→OAA) directions (Figure 2F). Recovery was most evident in PCK1 purified from cells exposed to glucose within the 15–25 mM range. SIRT2 did not restore PCK1 activity (Figures 2E and 2F). Similar results were obtained using overexpressed PCK1 from cells that co-overexpressed p300 (Figures 2G and 2H).

To investigate the role of p300 and SIRT1 in regulating PCK1 activity, we determined how overexpressing different combinations of PCK1, p300, and SIRT1 affected the gluconeogenic capacity of HEK293T cells in glucose-free media (Figures 2I, 2J, and S1C). Cells overexpressing PCK1 showed increased gluconeogenic activity after 6 hr (1.54 ± 0.09 μg/mg, n = 3, p = 0.0021) compared to control cells (0.96 ± 0.11 μg/mg), whereas those overexpressing both p300 and PCK1 did not (1.13 ± 0.06 μg/mg, n = 3, p = 0.0909). This result indicated that the ability of PCK1 to enhance gluconeogenesis was abolished when co-transfected with p300. Overexpression of PCK1 and SIRT1 (1.8 ± 0.3 μg/mg, n = 3, p = 0.0047) or PCK1, SIRT1, and P300 (2.3 ± 0.2 μg/mg, n = 3, p = 0.0061) yielded cells that produced similar amounts of glucose compared to that of cells overexpressing PCK1 alone. Collectively, these results suggested that dynamic acetylation of PCK1 modulates its activity under various glucose concentrations and is mediated by p300 and SIRT1.

## PCK1 Acetylation Enhances Its Anaplerotic Activity and Kinetically Disfavors the Gluconeogenic Reaction

To confirm that acetylation was the primary mechanism driving PCK1 activity, we utilized several different approaches. First, we analyzed the levels of acetylation at different glucose concentrations. PCK1 acetylation was higher under high glucose concentrations (Figure 3A), and inhibition of p300 with C646 yielded non-acetylated (Figure S2A) and fully active (Figure 2C) PCK1. To assess the proportion of acetylated PCK1 in cells, we determined site-specific acetylation stoichiometry using PCK1 purified from HEK293T cells and a previously described method (Baeza et al., 2014, 2015; Fan et al., 2016). PCK1 purified from HEK293T cells was incubated with either SIRT1 or SIRT2, and acetylation levels were compared to samples with only NAD$^+$ added. Only acetylation on Lys91 (~20% stoichiometry) was quantifiable (Figure 3B). *In vitro*, SIRT1, but not SIRT2, could deacetylate Lys91 of PCK1 (Figure 3B).

To understand how PCK1 activity is altered by acetylation, we analyzed the kinetic properties of PCK1 purified from HEK293T cells exposed to 10 mM (PCK1-10mM) and 15 mM (PCK1-15mM) glucose. Whereas no significant changes were observed in the kinetic properties for both OAA and GTP (Table S1A), PCK1-15mM showed decreased $K_m$ values for PEP (2.3-fold) and for GDP (2-fold). The catalytic efficiency ($k_{cat}/K_m$) was decreased (2-fold) in the OAA→PEP (gluconeogenic) reaction (Table S1A), while the PEP→OAA reaction was slightly improved (Table S1B). PCK1-10mM behaved almost identically compared to the recombinant form (Table S2). To confirm the role of SIRT1 in recovering PCK1 activity, PCK1-15mM samples were treated in the presence of recombinant purified sirtuins. SIRT1, but not SIRT2, treatment on PCK1-15mM samples was able to restore the kinetic properties of PCK1 (Table S1C).

Our results showed that acetylation directly affects the kinetic properties of PCK1 and that Lys91 was acetylated in HEK293T cells. Using Lys91 and lysine residues detected in other reports (Lundby et al., 2012; Weinert et al., 2013; Zhao et al., 2010), we mutated lysine 70, 71, 91, 124, 521, 524, and 594 to glutamine to create a potential acetyl-lysine mimic. K91Q substitution increased (3-fold) the $K_m$ value for PEP compared to wild-type (WT), while almost no effects were detected for the other K to Q mutants (Table S2). The observation that single K to Q substitutions did not mimic the phenotype of PCK1 purified from HEK293T suggested either acetylation had no effect on PCK1 activity or K to Q mutants were not mimicking an acetylated-lysine. To address this, we utilized a method to incorporate acetyl-lysine at specific sites encoding the amber termination codon (UAG) (Yu et al., 2012). Rat PCK1 and the acetyl-lysine-tRNAsynthetase (AcK-RS)/tRNA$^{CUA}$ were co-expressed in *E. coli* BL21 ΔCobB. We focused on residues close to the active site: Lys91, 521, and 524. Lys91 is located in the R-Loop and Lys521 and Lys524 are located in the GTP/GDP binding site of PCK1. A recent proteomic study also reported Lys473 acetylation (Shen et al., 2016). Lys473 is located in the Ω-Loop and was included here. Alignment of PCK1 sequences from different species indicated that Lys91, 473, and 521 were conserved (Figure S2B). Acetylation on K91, K473, and K521 (Figure S2C) improved the kinetic properties in the anaplerotic pathway (PEP→OAA) (Table S3B). PCK1 K91AcK and K473AcK variants had decreased (4.2 and 3.8-fold, respectively) $K_m$ values for PEP and showed increased (2.6- and 2-fold, respectively) catalytic efficiency ($k_{cat}/K_m$). Similarly, $K_m$ values for GDP, the nucleotide required for the conversion of PEP into OAA, of PCK1 K91AcK and K521AcK were decreased (4.4-fold in both cases), and $k_{cat}/K_m$ for this substrate was increased (5- and 4.4-fold, respectively). In the gluconeogenic reaction, K91AcK variant had decreased (20 and 25%) $k_{cat}$ values for OAA and GTP, respectively (Table S3A). Likewise, a decrease in $k_{cat}/K_m$ for OAA (30 and 10%, respectively) and GTP (25% in both cases) was observed for PCK1 K473AcK and PCK1 K521AcK, as a consequence of decreased $k_{cat}$ (20 and 35%, respectively) (Table S3A). Together, although K473AcK and K521AcK variants exhibited improved kinetic properties for one of the substrates (PEP and GDP, respectively) in the anaplerotic (PEP→OAA) reaction, PCK1 K91AcK catalyzed more efficiently both PEP and GDP, suggesting
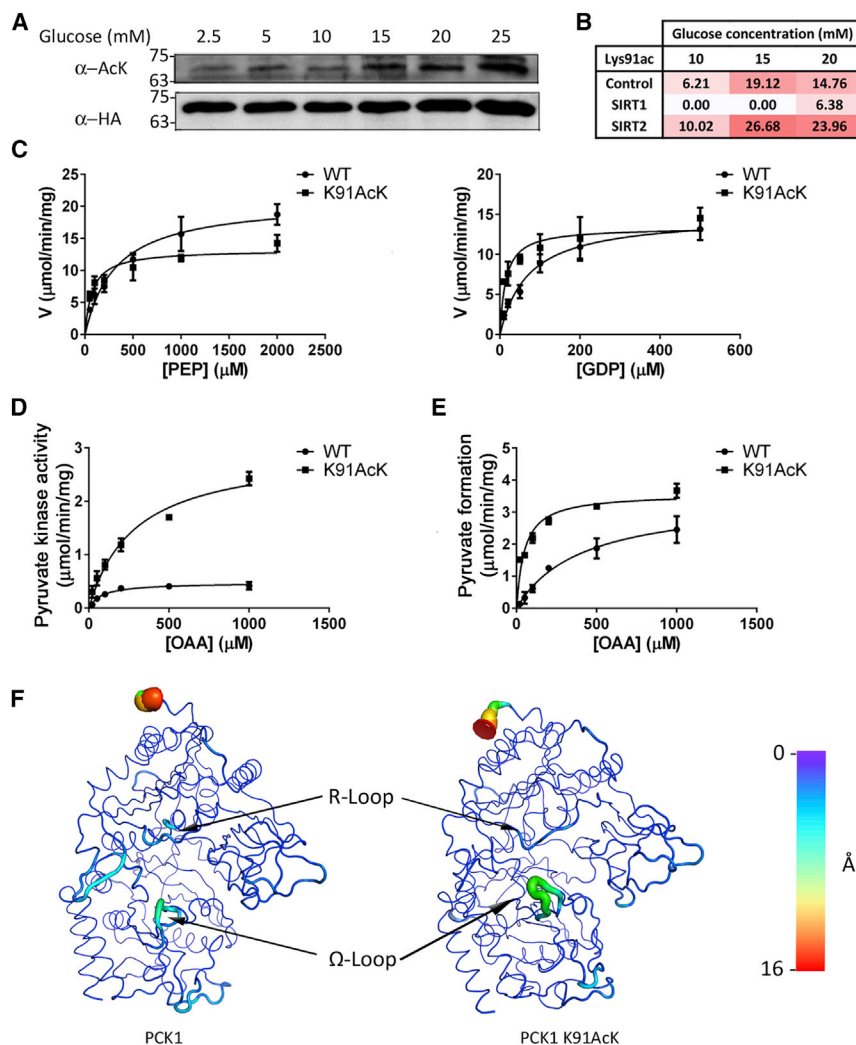
**Figure 3. Lys91 Acetylation Modifies PCK1 Activity**

(A) Glucose increases PCK1 acetylation. PCK1 acetylation was analyzed by western blot using samples from Figure 2A. Numbers indicate molecular weight (kDa) (see also Figure S2A and Table S1).

(B) Glucose determines PCK1 Lys91 acetylation level. PCK1 was purified from HEK293T exposed to different glucose concentrations. Prior to MS analysis, PCK1 was incubated in the presence of either SIRT1 (SIRT1) or SIRT2 (SIRT2). Acetylation stoichiometry is presented as percentage (%).

(C) Lys91ac increases catalytic efficiency for PEP and GDP. Comparative Michaelis-Menten plots for PEP, GDP, and $KHCO_3$ (see also Figures S2E and S2F and Tables S2 and S3).

(D) Lys91ac increases pyruvate kinase activity. Comparative Michaelis-Menten plot of pyruvate kinase activity (see also Figure S2G and Table S3C).

(E) Lys91ac destabilizes the closed-lid state of PCK1. Comparative Michaelis-Menten plot of enolate retention (see Figure S2H and Table S3D).(F) Lys91ac modifies the behavior of R-Loop and Ω-Loop. Atomic fluctuations of PCK1 (left) and K91AcK variant (right) (see also Figure S3 and Videos S1, S2, S3, and S4). Color bar represents distance (Å).

In (D) and (E), mean ± SD are represented, n = 3.

K521AcK mutants (Table S3D). Figures S2D–S2G show Michaelis-Menten plots for each substrate and acetylated variant.

Molecular dynamics (MD) simulations were performed to analyze the effects of Lys91 acetylation. In the absence of substrates, MD simulations revealed differential behavior of the R-Loop between PCK1 WT and PCK1 K91AcK (Figures 3F and S3; Videos S1 and S2). The flexibility of the Ω-Loop was also increased when Lys91 was acetylated (Figure S3; Videos S1 and S2), a change that was also observed in the simulations performed in the presence of oxalate and GTP (Figure S3; Videos S3 and S4). Lys91 lies in the R-loop whose coordination with the Ω-loop of PCK1 is essential for catalysis (Johnson et al., 2016). These MD simulations provide physical evidence that acetylation of Lys91 leads to altered dynamics of the substrate binding regions, which alter substrate interactions to disfavor the gluconeogenic reaction.

Next, we investigated whether PCK1 is able to perform the reverse reaction (PEP→OAA) in cells under high glucose. Metabolomic tracing experiments were performed using HEK293T cells incubated in the presence of either $^{13}C_6$-glucose or $^{13}C_3$-pyruvate as tracers. Because the PCK1 reverse reaction would likely be masked by the activity of pyruvate carboxylase (PC), a major anaplerotic enzyme that transforms pyruvate into OAA (Jitrapakdee et al., 2006; Owen et al., 2002), the experiments were performed in cells in which PC was knocked down using small interfering RNA (siRNA). Surprisingly, PCK1

that Lys91 acetylation potentiates PCK1 anaplerotic activity (Table S3B; Figure 3C). Gel filtration chromatography indicated that PCK1 K91AcK was monomeric, similar to unmodified PCK1 (Figure S2D). Except for K524AcK, acetylation on Lys91, 473, and 521 turned the gluconeogenic (OAA→PEP) reaction unfavorable (Table S3). It is known that PCK1 exhibits pyruvate kinase (PK) activity that increases with mutations affecting the active-site structure (Johnson et al., 2016). We used this PK activity to probe alterations in the active site. K91AcK showed higher (5-fold) PK activity (Table S3C; Figure 3D), as was also observed for K473AcK and K521AcK variants (Table S3C), indicating alterations of the catalytic site. We also assessed the ability of the acetylated variants to maintain the integrity of the enolate intermediate by performing the PK reaction in the absence of a phosphoryl donor (GDP instead of GTP) (Johnson and Holyoak, 2010; Johnson et al., 2016). With the altered active site, the PK reaction of PCK1 is blocked, and the enolate is more easily transformed into pyruvate by spontaneous protonation. In PCK1 K91AcK, the $k_{cat}/K_m$ value for this reaction was 9-fold higher than that of WT (Table S3D; Figure 3E). A minor effect was seen in the K473AcK and
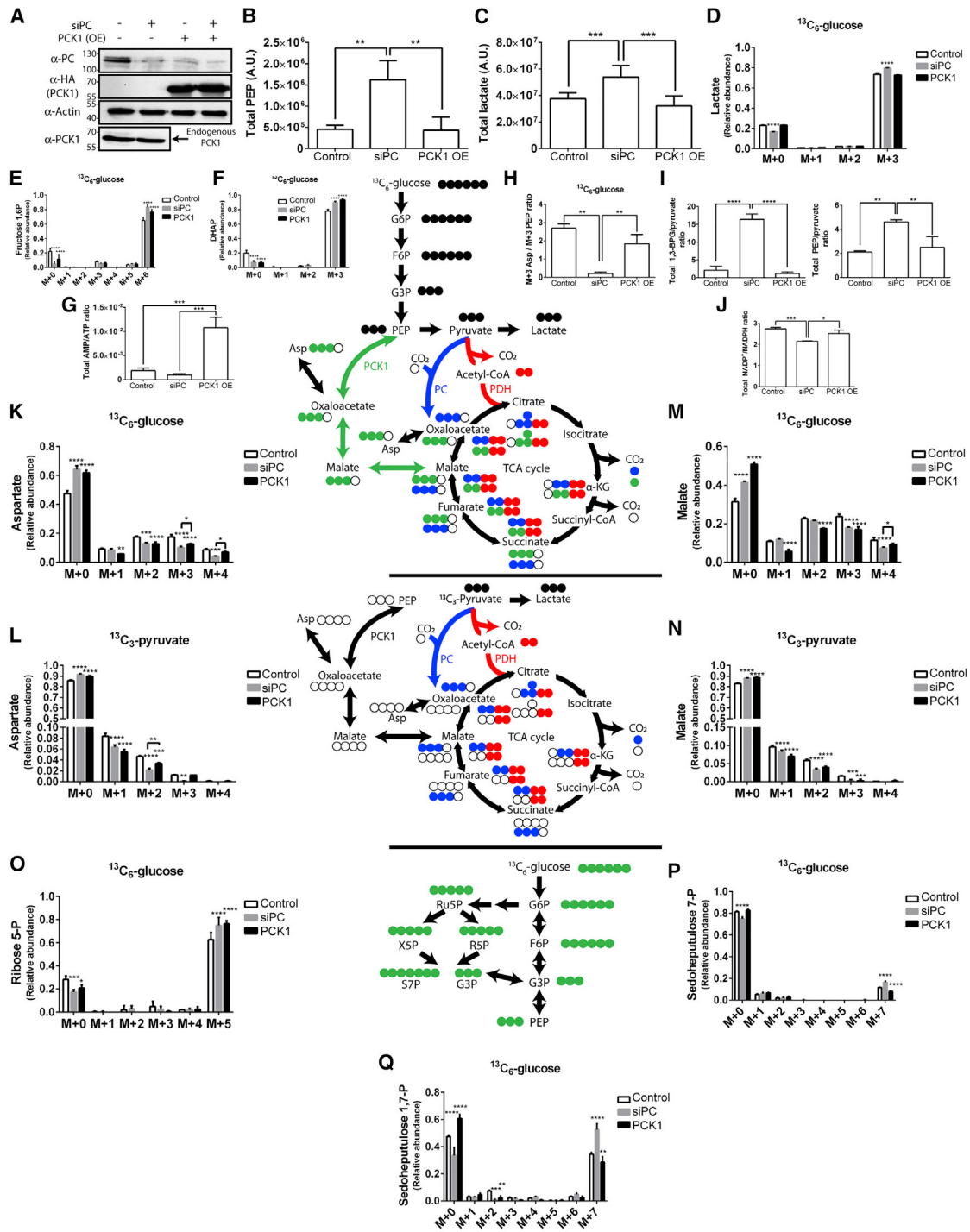
**Figure 4. PCK1 Is Able to Perform Its Reverse (PEP→OAA) Reaction in HEK293T Cells**

(A) PCK1 overexpression leads to PC downregulation. HEK293T cells were transfected with either PCK1 construct or siPC oligos or both, and protein expression of PC (α-PC), overexpressed PCK1 (α-HA), and endogenous PCK1 (α-PCK1) were checked by western blotting. Numbers on the left represent molecular weight (kDa), n = 3.

(B–D) PC silencing leads to PEP accumulation and promotes lactate metabolism. Total levels of PEP (B) or lactate (C) and $^{13}C$ isotopomer distribution of lactate (D).

(E and F) PCK1 promotes glucose utilization. $^{13}C$ isotopomer distribution of fructose 1,6-biphosphate (E) and DHAP (F) using $^{13}C_6$-glucose as tracer.

(G) PCK1 overexpression increases AMP/ATP ratio. Total AMP/ATP ratio.

*(legend continued on next page)*

overexpression alone induced a dramatic downregulation of PC protein levels similarly to PC siRNA oligos (Figure 4A). Cells over-expressing PCK1 at the same time PC was silenced displayed an abnormal growth as clumps instead of a monolayer and there-fore were excluded from the metabolomics analyses. We initially observed that PC silencing significantly increased total levels of PEP (3.6-fold, n = 3, p = 3.9 × 10$^{-5}$) (Figure 4B). Nevertheless, in the context of loss of PC, overexpression of PCK1 restored PEP levels (Figure 4B) compared to controls. Additionally, the signif-icant increase (44%, n = 3, p = 3.2 × 10$^{-3}$) in lactate metabolism due to PC silencing was corrected when PCK1 was overex-pressed (Figure 4C). This is also evident from the increase in the relative abundance of M+3 and the decrease of M+0 lactate isotopomers when PC was silenced, using $^{13}C_6$-glucose as tracer (Figure 4D). Compared to controls, the increase in the rela-tive abundance of glycolysis intermediates such as M+6 fructose 1,6-bisphosphate (Figure 4E) and M+3 dihydroxyacetone phos-phate (DHAP) (Figure 4F) suggest that PCK1 promotes glucose utilization, as previously reported (Montal et al., 2015). This is supported by the 6-fold (n = 3, p = 0.004) increase in the AMP/ATP ratio (Figure 4G), which is an indicator of cellular energy status (Hardie, 2004). An increase in the AMP/ATP ratio due to PCK1 overexpression activates AMPK in *C. elegans* (Yuan et al., 2016). This activation promotes catabolism to stimulate ATP production and inhibits anabolism (Herzig and Shaw, 2018), favoring the supply of PCK1 reverse reaction substrates.

We then assessed metabolic hallmarks providing evidence of PCK1 reverse reaction and analyzed aspartate and malate labeling. OAA is very unstable, and we were unable to detect suf-ficient levels for quantitation, but the conversion of OAA to aspar-tate by aspartate aminotransferase offers an indirect way to assess OAA labeling. We observed that PCK1 overexpression rescued the M+3 aspartate/M+3 PEP ratio, which was dramati-cally decreased (90% compared to controls, n = 3, p = 0.0022) when PC was silenced (Figure 4H). In contrast, the increase in 1,3-bisphosphoglycerate/pyruvate (8-fold, n = 3, p = 7.3 × 10$^{-5}$) and PEP/pyruvate (2-fold, n = 3, p = 0.0026) ratios due to PC silencing was corrected when PCK1 was overexpressed in the context of loss of PC (Figure 4I). Additionally, the decrease in the redox NADP$^+$/NADPH ratio due to PC silencing (20% of con-trols, n = 3, p = 0.0009) was rescued when overexpressing PCK1 (Figure 4J) in the context of PC downregulation. PCK1 overex-pression partly recovered the relative abundance of M+3 aspar-tate derived from $^{13}C_6$-glucose and lost by PC downregulation (Figure 4K). In full agreement, the decrease in M+2 and the in-crease in M+3 and M+4 aspartate suggest that PCK1 is able to perform the reverse reaction and to provide intermediates for the TCA cycle in the context of loss of PC. This was also supported by the fact that PCK1 overexpression led to an increase in the relative abundance of M+2 aspartate derived from $^{13}C_3$-pyruvate compared to the PC silencing condition (Figure 4L), although this labeling does not exclude other metabolite sources. Additionally, PCK1 overexpression was able to rescue the relative abundance of M+4 malate in the context of PC downregulation when derived from $^{13}C_6$-glucose (Figure 4M), and, although no significant changes were seen for M+2 and M+4 malate derived from $^{13}C_3$-pyruvate between PC silencing and PCK1 overexpressing conditions, we did observe a decrease in M+3 malate due to PCK1 overexpression (Figure 4N), compared to controls. The latter was similar to the PC silencing condition, suggesting a loss of PC activity. Collectively, the aspartate and malate labeling is consistent with PCK1 running the reverse reaction in cells, but the increase in the relative abundance of M+0 metabolites also indicated an influx from carbon sources other than glucose.

PCK1 overexpression also led to an increase in the relative abundance of M+5 ribose 5-phosphate (Figure 4O), suggesting an increase into the pentose phosphate pathway (PPP), but the low label into nucleotides would indicate nucleotide synthesis is inhibited. This inhibition is evident from M+7 labeling of sedoheptulose 7-phosphate (Figure 4P) and its precursor sedo-heptulose 1,7-biphosphate (Figure 4Q). Ribose-5-phosphate is a substrate inhibitor of transketolase (Solovjeva et al., 2016), which takes xylulose 5-phosphate and ribose 5-phosphate to generate sedoheptulose 7-phosphate and glyceraldehyde 3-phosphate (G3P), which is interconverted to DHAP. Ribose 5-phosphate in-hibits the synthesis of phosphoribosylpyrophosphate (PRPP) (Switzer and Sogin, 1973), which is required for nucleotide synthe-sis and might explain the lower incorporation of M+5 label into nucleotides. Together, our results suggest that PCK1 anaplerotic activity is possible in PC-downregulated HEK293T cells and cor-rects the metabolic defects of loss of PC and fuels the TCA cycle activity by providing metabolites and by promoting the utilization of metabolites others than glucose as a carbon source.

### SIRT1 Deacetylates PCK1 *In Vivo* and *In Vitro*

To provide evidence for the direct functional interaction between SIRT1 and PCK1, we performed additional analyses in cultured cells and *in vivo*. PCK1 from HEK293T cells (PCK1-10mM and PCK1-15mM samples) was incubated in the presence of either human recombinant SIRT1 or SIRT2, and the acetylation level was evaluated by western blotting. SIRT1, but not SIRT2, was able to deacetylate PCK1 under these conditions (Figure 5A), consistent with the MS results (Figure 3B). PCK1 was overex-pressed alone or in the presence of either SIRT1 or SIRT1 H363Y deacetylation-deficient mutant. Western blot analysis of immuno-purified PCK1 indicated that overexpression of SIRT1 reduced the level of acetylation of PCK1 in HEK293T cells (Figure 5B).

(H–J) PCK1 overexpression restores metabolite ratios in the cell. M+3 Asp/M+3 PEP from 13C isotopomer (H) and total metabolite ratios: 1,3-BPG/pyruvate (I, left), PEP/pyruvate (I, right) and NADP+/NADPH (J). Asp, aspartate; PEP, phosphoenolpyruvate; 1,3-BPG, 1,3 biphosphoglycerate; pyr, pyruvate.
(K–N) PCK1 reverse reaction is possible in HEK293T cells. $^{13}C$ isotopomer distribution of aspartate (K and L) and malate (M and N) using either $^{13}C_6$-glucose (K and M) or $^{13}C_3$-pyruvate (L and N) as tracers.
(O–Q) PCK1 overexpression inhibits the pentose phosphate pathway (PPP). $^{13}C$ isotopomer distribution of ribose 5-phosphate (O), sedoheptulose 7-phosphate (P), and sedoheptulose 1,7-biphosphate (Q) using $^{13}C_6$-glucose as tracer.
In (B)–(Q), mean ± SD are represented, *p < 0.05; **p < 0.01; ***p < 0.001; ****p < 0.0001, n = 3. Statistical differences are referred to controls (control versus siPC and control versus PCK1 OE). Only those comparisons highlighted in the main text between siPC and PCK1 OE conditions are represented.
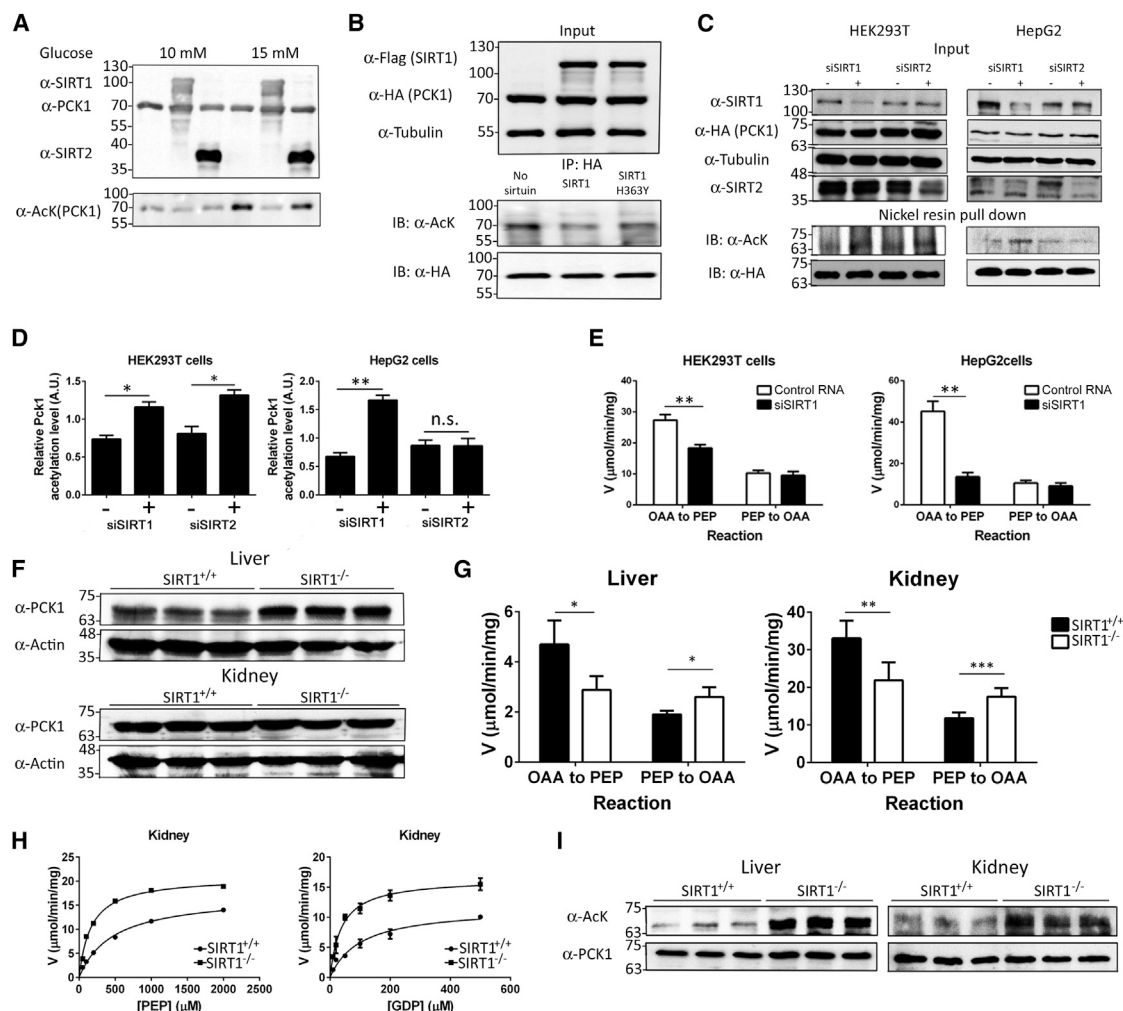
**Figure 5. PCK1 Is a SIRT1 Substrate *In Vitro* and *In Vitro***

(A) SIRT1 deacetylates PCK1 *in vitro*. PCK1 was purified from HEK293T cells exposed to different glucose concentrations and treated with either recombinant SIRT1 or SIRT2 deacetylases.

(B) Overexpression of SIRT1 decreases PCK1 acetylation level. PCK1 and either SIRT1 WT or SIRT1 H363Y inactive mutant were co-expressed in HEK293T. PCK1 was immunoprecipitated from HEK293T lysates and probed using anti-acetyl-lysine (AcK) antibody, n = 3.

(C) SIRT1 silencing increases PCK1 acetylation in both HEK293T and HepG2 cells. Both SIRT1 (siSIRT1) and SIRT2 (siSIRT1) were silenced in both gluconeogenic cell lines and PCK1 was pulled down using nickel resin and probed using an anti-acetyl-lysine (AcK) antibody, n = 2 (see also Figure S4A).

(D) Quantification of the relative level of acetylation of PCK1 obtained from (C). Mean ± SD, n = 2.

(E) Silencing SIRT1 modifies PCK1 activity. The activity of PCK1 obtained from (C) was determined in both reaction directions. White bars, PCK1 obtained from cells normally expressing SIRT1. Black bars, PCK1 purified from SIRT1 knockdown cells. Mean ± SD, n = 2, **p < 0.01.

(F) Expression levels of PCK1 from WT ($SIRT1^{+/+}$) and SIRT1 KO ($SIRT1^{-/-}$) tissues, n = 3.

(G) Activity of PCK1 purified from animals from (F) was measured in both reaction directions (see Figure S4B and Table S4). Mean ± SD, n = 3, *p < 0.05, **p < 0.01, ***p < 0.001.

(H) Comparative Michaelis-Menten plots of PCK1 purified from WT ($SIRT1^{+/+}$) and SIRT1 KO ($SIRT1^{-/-}$) tissues for PEP and GDP. Mean ± SD, n = 3 (see Table S4).

(I) SIRT1 is a PCK1 deacetylase in mice. Acetylation level of PCK1 purified from (F) determined by western blotting.

To determine whether endogenous SIRT1 or SIRT2 regulates the acetylation level of PCK1, specific siRNA oligos targeting either SIRT1 or SIRT2 mRNA were used. In HEK293T cells, silencing SIRT1 or SIRT2 increased PCK1 acetylation levels (n = 2; p = 0.0182 and p = 0.02951, respectively), whereas with HepG2 cells, acetylation increased only when silencing SIRT1 (n = 2, p = 0.0069) (Figures 5C and 5D). In HepG2 cells, endogenous PCK1 levels decreased approxi-

mately 50% when silencing SIRT1 (Figure S4A), consistent with a previous report (Lin et al., 2009). Analysis of PCK1 activity purified from SIRT1 knockdown cells indicated that the gluconeogenic activity (OAA→PEP reaction) of PCK1 was decreased in HEK293T and HepG2 cells (~40% and 70% of control, respectively), whereas no changes in PCK1 activity were observed for the reverse reaction (PEP→OAA) (Figure 5E).
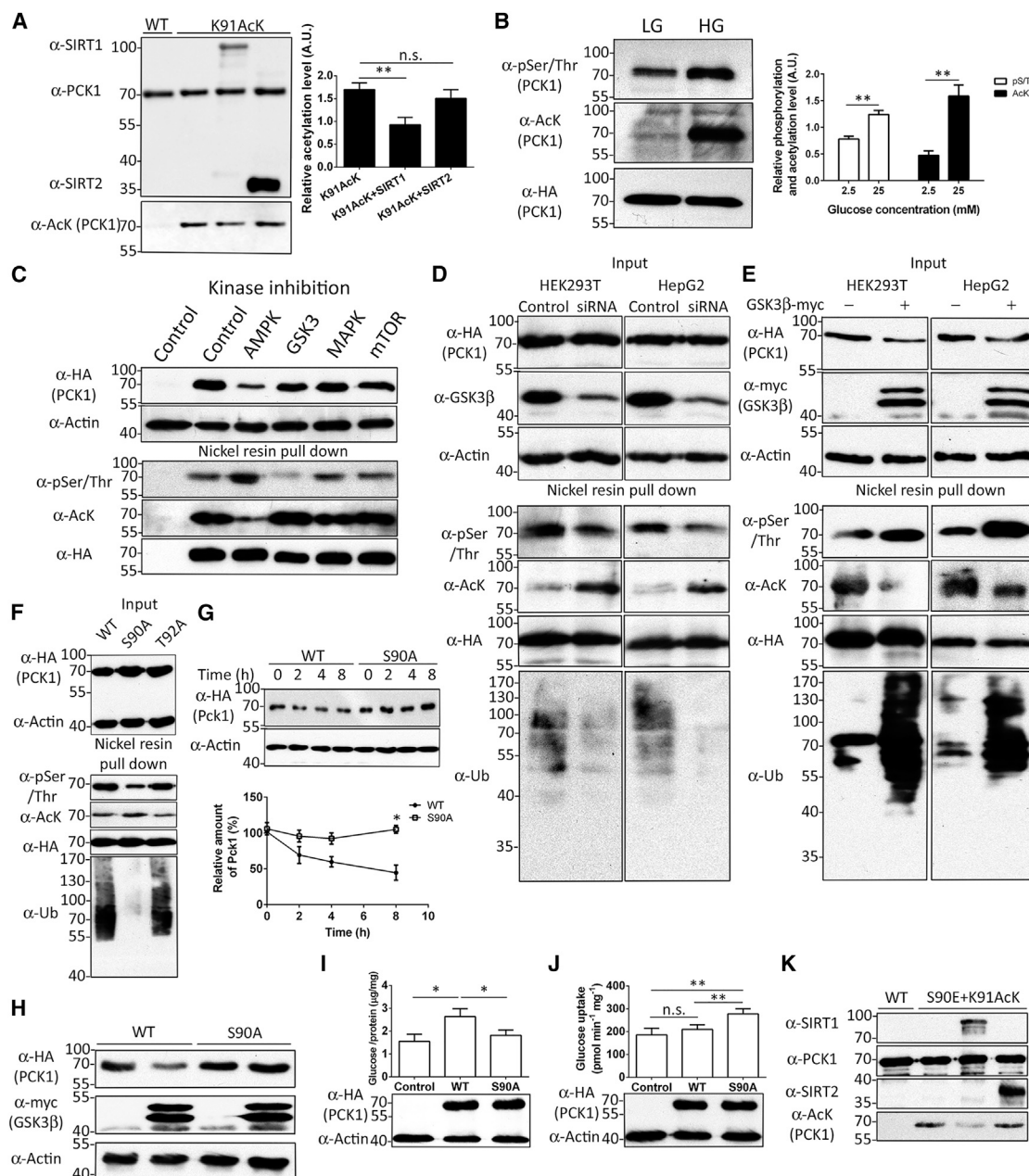
**Figure 6. GSK3β-Mediated Phosphorylation Controls PCK1 Stability and Facilitates SIRT1-Dependent Deacetylation**

(A) SIRT1 partially deacetylates recombinant PCK1 K91AcK *in vitro* in the presence of 2 mM NAD⁺. Relative acetylation levels in the absence (K91AcK) or in the presence of SIRT1 (K91Ack+SIRT1) or SIRT2 (K91AcK+SIRT2). Mean ± SD, n = 3, **p < 0.01.

(B) PCK1 (α-HA) was pulled down from HEK293T cells exposed to low- (LG; 2.5 mM) or high-glucose (HG; 25 mM) media and its phosphorylation and acetylation were determined using. Graphs on the right represent mean ± SD, n = 3.

(C) AMPK and GSK3 inhibition affects PCK1 phosphorylation and acetylation. HEK293T cells overexpressing PCK1 (α-HA) were treated with different kinase inhibitors. PCK1 was pulled down and its acetylation and phosphorylation levels were analyzed (see Figures S5A–S5C).

(D) Silencing GSK3β decreases PCK1 phosphorylation and ubiquitination and increases its acetylation. Endogenous GSK3β was silenced (siGSK3β) in cells overexpressing PCK1 (α-HA). PCK1 was pulled down and analyzed by western blot, n = 2.

(E) Overexpression of GSK3β increases PCK1 phosphorylation (α-pSer/Thr) and ubiquitination (α-Ub) and decreases acetylation (α-AcK) in HEK293T and HepG2 cells. PCK1 (α-HA) was pulled down and probed against different PTMs, n = 2 (see also Figures S5D and S5E).

(F) S90A substitution decreases phosphorylation (α-pSer/Thr) and ubiquitination (α-Ub) and increases acetylation (α-AcK) of PCK1. Phosphorylation and acetylation of pulled down PCK1 WT, PCK1 S90A (S90A), and PCK1 T92A (T92A) were determined, n = 3 (see also Figure S5F).

(G) S90A substitution increases PCK1 half-life. HEK293T overexpressing PCK1 WT or PCK1 S90A (S90A) were treated with cycloheximide and harvested at different time points, mean ± SD, n = 2, *p < 0.05.

*(legend continued on next page)*

Next, we evaluated *in vivo* the regulation of PCK1 by acetylation. Endogenous PCK1 was partially purified from mouse WT (*Sirt*$^{+/+}$) and SIRT1 knockout (KO) (*SIRT1*$^{-/-}$) liver and kidney (Figure S4B). Though the endogenous levels of PCK1 were similar in kidney from WT and KO, the levels of mouse PCK1 in livers from WT animals were lower than those from *SIRT1*$^{-/-}$ mice (Figure 5F), in agreement with another report (Wang et al., 2011). PCK1 from *SIRT1*$^{-/-}$ mice exhibited lower activity (30%–40%) in the OAA→PEP direction but higher (30%–35%) in the PEP→OAA reaction in both liver and kidney (Figure 5G; Table S4A). In addition, PCK1 from *SIRT1*$^{-/-}$ mice showed lower $K_m$ values (2.6- and 2.8-fold for PEP and GDP, respectively), higher $k_{cat}$ values (25% and 20% for PEP and GDP, respectively) and in turn an increase in catalytic efficiency by 3.5-fold (Figure 5H; Table S4B) compared to WT. Finally, PCK1 from *SIRT1*$^{-/-}$ mice showed higher acetylation levels compared to controls (Figure 5I). Taken together, our results demonstrated that SIRT1 directly regulates PCK1 via deacetylation *in vitro* and *in vivo* and confirmed that increased acetylation disfavors the PCK1 gluconeogenic reaction and that acetylation promotes the reverse anaplerotic reaction.

## GSK3β Mediates PCK1 Phosphorylation

Although our results demonstrated that SIRT1 deacetylated PCK1 purified from mammalian cells, recombinant bacterially expressed PCK1 K91AcK was recalcitrant to complete deacetylation *in vitro*. Purified SIRT1 was able to deacetylate ~50% of the purified PCK1 K91AcK in the presence of 2 mM NAD$^+$ (Figure 6A). Though we could not rule out the possibility that ~50% of the recombinant bacterially expressed PCK1 K91AcK was denatured, and therefore the K91 site was occluded to SIRT1, we asked whether PCK1 (from mammalian cells) might be post-translationally modified by another modification, such as phosphorylation, and this form of PCK1 might be a better substrate for SIRT1. Several proteomic studies have reported Ser/Thr phosphorylation on different residues of PCK1 in gluconeogenic tissues from mouse (Grimsrud et al., 2012; Parker et al., 2015; Robles et al., 2017; Wilson-Grady et al., 2013), rat (Demirkan et al., 2011; Lundby et al., 2012), and human (Bian et al., 2014). Given the fact that Lys91 is bookended by two conserved residues, Ser90 and Thr92 (see Figure S2B), we hypothesized that phosphorylation on those residues can affect PCK1 deacetylation.

First, we determined whether PCK1 was phosphorylated by performing pull-down assays using lysates from HEK293T cells exposed to different glucose concentrations. Ser/Thr phosphorylation of PCK1 was measurable at high and low glucose but was significantly higher (1.6-fold, n = 3, p = 0.0017) under high glucose conditions (Figure 6B). When the same samples were analyzed for acetylation, high glucose induced a large (3.4-fold, n = 3, p = 0.0055) increase in acetylation (Figure 6B), indicating that high-glucose conditions lead to both hyperphosphorylation and -acetylation of PCK1.

To identify candidate kinases, PCK1 was analyzed from cells exposed to different kinase inhibitors. Due to their role in regulating PCK1 expression, and thus gluconeogenesis, AMPK (Horike et al., 2008), GSK3 (Lipina et al., 2005), MAPK (Xu et al., 2005), and mTOR (Khan et al., 2015) were selected for chemical inhibition. AMPK inhibition decreased the levels of overexpressed PCK1 down to 68% of control (n = 3, p = 0.0302, Figure S5A), increased PCK1 phosphorylation (1.5-fold, n = 4, p = 0.0131), and decreased (2-fold, n = 4, p = 0.0045) PCK1 acetylation level compared to those of control cells (Figure 6C). GSK3 inhibition decreased (2.5-fold, n = 4, p = 0.0011) PCK1 phosphorylation, and dual inhibition of AMPK and GSK3 did not affect the levels of overexpressed PCK1. A similar effect was obtained when replacing the GSK3 inhibitor with the proteasome inhibitor MG132 (Figures S5B and S5C). Inhibition of either MAPK or mTOR did not yield any significant effect on PCK1 protein or post-translational modification (PTM) levels (Figures 5C and S5A).

The AMPK inhibitor dorsomorphin can also inhibit AKT (Liu et al., 2014), which phosphorylates and inhibits GSK3 (Beurel et al., 2015). Inhibition of AMPK would also inhibit AKT and thus yield a hyperactive GSK3. To test this hypothesis, we first silenced GSK3β, which also regulates PCK1 transcriptionally (Horike et al., 2008). Figure 6D shows that GSK3β silencing decreases PCK1 phosphorylation and ubiquitination and increases PCK1 acetylation in both HEK293T and HepG2 cells. In the complementary experiment, co-overexpression of GSK3β and PCK1 increased PCK1 phosphorylation and ubiquitination, and decreased acetylation (Figure 6E). GSK3β overexpression decreased the levels of PCK1 by a half in both cell lines. The observation that recombinant GSK3β could not phosphorylate PCK1 *in vitro* (Figure S5D) and that no GSK3β was co-purified by pull-down assays (Figure S5E) suggested that GSK3β does not directly phosphorylate PCK1, but that GSK3β is upstream of a pathway required to phosphorylate PCK1.

We tested the hypothesis that Ser90 and Thr92 of PCK1 are phosphorylated and that there is crosstalk between acetylation, phosphorylation, and ubiquitination. We analyzed the level of phosphorylation and acetylation of purified PCK1 WT and mutants S90A and T92A. The PCK1 S90A mutant had decreased (55%, n = 3, p = 0.017) phosphorylation and increased (30%, n = 3, p = 0.019) acetylation levels (Figures 6F and S5F). Additionally, the S90A mutant was less ubiquitinated (Figure 6F). Compared to WT, the S90A substitution increased the half-life of PCK1 (Figure 6G). Overexpression of GSK3β did not affect

(H) PCK1 S90A levels remain constant in the presence of GSK3β. PCK1 WT or S90A (α-HA) mutant were independently expressed in the presence or in the absence of overexpressed GSK3β (α-myc), n = 2.

(I) S90A substitution reduces PCK1 gluconeogenic ability. The gluconeogenic ability of PCK1 (WT) or PCK1 S90A (S90A) (α-HA) was determined in HEK293T. *p < 0.05, n = 3.

(J) S90A substitution promotes glucose uptake in HEK293T cells. Glucose uptake rates were determined for mock-transfected cells (Control) and cells overexpressing either PCK1 (WT) or PCK1 S90A (S90A). **p < 0.01, n = 4, n.s., not significant. In (I) and (J), a representative western blot is presented below each graph.

(K) PCK1 S90E+K91AcK is deacetylated by SIRT1 *in vitro* in the presence of 0.5 mM NAD$^+$ (see Figures S5G–S5I).
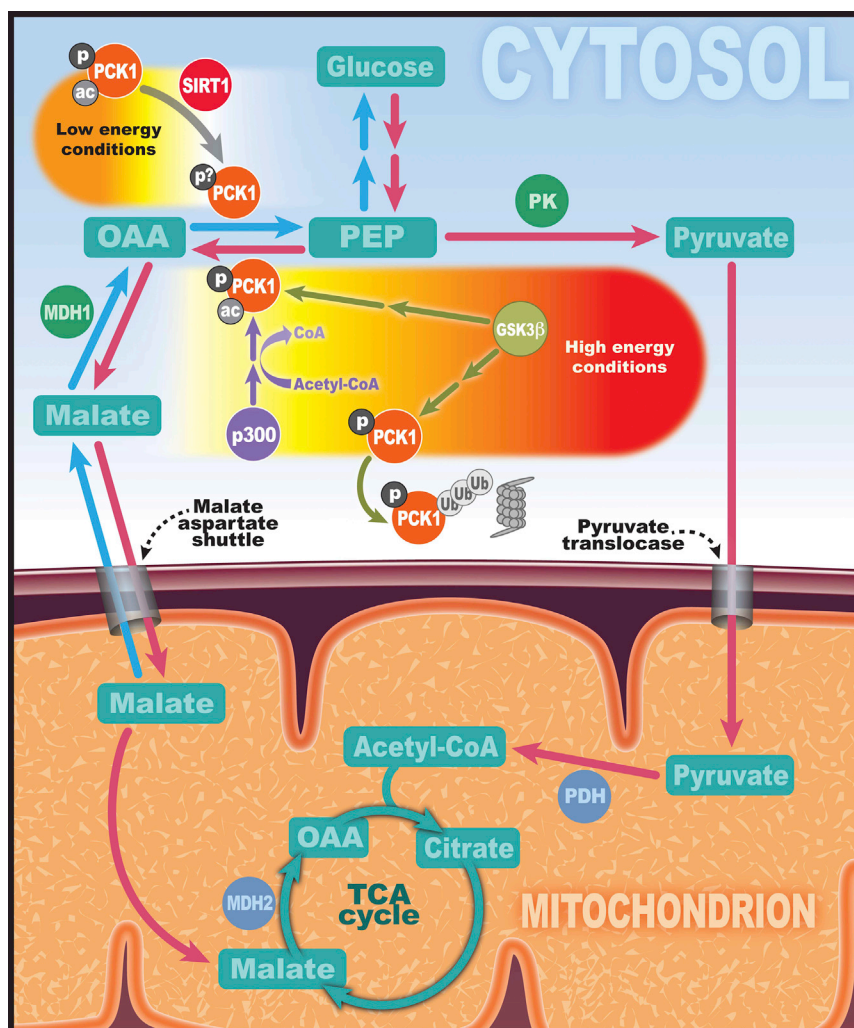
**Figure 7. Schematic Representation of the Role of Acetylation, Phosphorylation, and Ubiquitination in Regulating PCK1 Activity**
The glycolytic (red arrows) and gluconeogenic (blue arrows) pathways are represented. SIRT1, Sirtuin 1; PCK1, cytosolic phosphoenolpyruvate carboxykinase; MDH1/2, cytosolic/mitochondrial malic dehydrogenase; PK, pyruvate kinase; PDH, pyruvate dehydrogenase complex; p300, acetyltransferase p300. Acetylation (Ac), phosphorylation (P), and ubiquitination (Ub) are represented.

evidence that the dually acetylated and phosphorylated form of PCK1 is the preferred target for SIRT1-dependent PCK1 K91AcK deacetylation. The implications of this complex PTM crosstalk are discussed below.

## DISCUSSION

At high glucose, PCK1 acetylation by p300 promotes PCK1 anaplerotic activity (PEP→OAA), where acetylation of Lys91 favors anaplerotic activity by improving the kinetic properties for PEP and GDP, and concomitantly turning the gluconeogenic pathway kinetically unfavorable. Under low glucose, p300 activity is decreased, and SIRT1 levels rise to deacetylate PCK1, restoring the gluconeogenic ability of PCK1 (Figure 7). GSK3β-mediated phosphorylation promotes PCK1 ubiquitination and degradation at high glucose and in context-specific fashion. Serine phosphorylation

PCK1 S90A levels (Figure 6H), while GSK3β did induce the degradation of WT PCK1. The analysis of functional properties revealed that the gluconeogenic ability of PCK1 S90A variant was significantly reduced (31%, $1.8 \pm 0.2$ μg/mg, n = 3, p = 0.023) compared to PCK1 WT ($2.6 \pm 0.3$ μg/mg) (Figure 6I). However, cells overexpressing PCK1 S90A showed significantly higher glucose uptake rates ($278 \pm 23$ pmol min$^{-1}$ mg$^{-1}$) compared to control cells ($186 \pm 29$ pmol min$^{-1}$ mg$^{-1}$, 1.5-fold, p = 0.0031, n = 4) and to cells overexpressing PCK1 WT ($210 \pm 21$ pmol min$^{-1}$ mg$^{-1}$, 1.3-fold, p = 0.0048, n = 4) (Figure 6J).

To mimic phosphorylation at S90 and assess the ability of SIRT1 to deacetylate K91AcK, we generated a variant of PCK1 that contains the S90E substitution and has the K91AcK installment. The purified PCK1 S90E+K91AcK double variant was expressed and purified from *E. coli*. SIRT1 completely deacetylated this PCK1 variant (Figures 6K, S5G, and S5H) in the presence of 0.5 mM NAD$^+$ and restored kinetic properties similar to WT (Figure S5I; Table S4C). Altogether, these results identify a novel GSK3β-dependent pathway that phosphorylates PCK1 under high glucose and suggest that phosphorylated PCK1 is the form targeted for ubiquitin-based degradation and provide

adjacent to Lys91 facilitates SIRT1-dependent deacetylation of PCK1 under low-energy conditions. Together, our results show that acetylation triggers PCK1 anaplerotic activity and that the interplay between acetylation, phosphorylation, and ubiquitination controls PCK1 in central metabolic pathways (Figure 7).

PCK1 catalyzes a rate-limiting step of gluconeogenesis forming PEP from OAA (Yang et al., 2009a). Hyperacetylated PCK1 favors the reverse reaction, and sustained hyperacetylation of PCK1 might explain a key mechanistic contribution of PCK1 in diabetes (Beale et al., 2004, 2007) and cancer, where the anabolic capacity from glutamine and the utilization of glucose of human PCK1 are implicated in tumor growth (Montal et al., 2015). The relatively long half-life of PCK1 in rat tissues (Hopgood et al., 1973), and data reported here support a possible role of PCK1 during glycolysis. PCK1 homologs from yeast and bacteria display anaplerotic activity: *S. cerevisiae* (Zelle et al., 2010), ΔCobB *S. enterica* (Wang et al., 2010), and *E. coli* (Fuhrer et al., 2005), when glucose was the carbon source. PCK1 purified from mammalian gluconeogenic cells under high glucose showed diminished activity in the gluconeogenic pathway (Figure 2). Acetylation of Lys91 improves the catalytic efficiency for

PEP and GDP in the anaplerotic reaction (Table S3). While SIRT1 can modulate the expression of gluconeogenic genes (Caton et al., 2011; Rodgers and Puigserver, 2007; Rodgers et al., 2005), results here demonstrate a more immediate role of SIRT1 in deacetylating PCK1 and favoring gluconeogenesis under low-energy input. High TCA flux activity (Satapati et al., 2012; Sunny et al., 2011) has been observed in SIRT1 deficient mice (Purushotham et al., 2009). During the fed state, upregulated MDH1 (Kim et al., 2012; Zhao et al., 2010) and MDH2 (Yang et al., 2015, 2011) would facilitate the incorporation of the OAA generated by PCK1 from cytosol into the TCA cycle as malate (Figure 7). In the context of diabetes-induced hyperacetylation (Kosanam et al., 2014), acetylated PCK1 might promote glycolysis, reducing glycemic load. Under high-energy conditions, both PCK1 and mitochondrial PCK2 would coordinate metabolite homeostasis between the cytosol and the mitochondrion (Figure 7). During fasting, SIRT1 restores the full kinetic properties of PCK1 in gluconeogenic tissues to promote its gluconeogenic activity. Together, these observations indicate that the conversion of PEP into OAA can occur *in vivo*, providing key evidence that PCK1 harbors metabolic functions beyond gluconeogenesis in mammals.

We show that phosphorylation of PCK1 was GSK3β dependent and increased PCK1 ubiquitination and degradation (Figure 6), indicating a dual role of GSK3β in regulating PCK1 at the level of protein turnover and gene expression (Horike et al., 2008). GSK3β-dependent phosphorylation of Ser90, adjacent to Lys91, was critical for PCK1 stability and suggested an interplay between PCK1 phosphorylation and acetylation. Although high glucose can induce PCK1 degradation through the GSK3β pathway (Figure 6), PCK1 degradation *in vivo* is relatively slow, acting after several hours of high glucose (Tilghman et al., 1974). High glucose also induced an increase in PCK1 phosphorylation and acetylation. We propose that high glucose triggers acetylation by p300, and in a context-specific manner, GSK3β-dependent phosphorylation. The cell attempts to integrate these signals, perhaps dependent on the length of high glycemic load, and prime the PTM state of PCK1 for slow degradation (via sustained phosphorylation), or for more rapid deacetylation via SIRT1 upon the next fasted state. Interestingly, *in vivo* ubiquitination of many PCK1 lysines has been reported (Wagner et al., 2012) including Lys91 and others such as Lys71 or Lys124 that can also be acetylated (Wang et al., 2010; Weinert et al., 2013). This suggests a competitive mechanism between acetylation and ubiquitination. The inefficient SIRT1-dependent deacetylation of bacterially expressed PCK1 was noted by Knyphausen et al. (2016) who reported this recalcitrant deacetylation at positions 70, 71, and 594. Knyphausen et al. did not observe deacetylation until they mutated nearby residues to acidic groups, which mimicked a robust deacetylation site on a different protein. Here, we show that mammalian-expressed PCK1 can be deacetylated and that PCK1 K91AcK is more efficiently deacetylated by SIRT1 when a phospho-mimetic S90E+K91AcK variant was utilized, restoring the gluconeogenic ability of PCK1. In conclusion, our results reveal that an interplay between phosphorylation, acetylation, and ubiquitination, which is regulated by p300, SIRT1, and GSK3β, controls PCK1 activity in anaplerotic and cataplerotic metabolism in response to energy input.

## STAR★METHODS

Detailed methods are provided in the online version of this paper and include the following:

- KEY RESOURCES TABLE
- CONTACT FOR REAGENT AND RESOURCE SHARING
- EXPERIMENTAL MODEL AND SUBJECT DETAILS
  - SIRT1$^{+/+}$ and SIRT1$^{-/-}$ mice
  - Cell cultures
- METHOD DETAILS
  - Determination of endogenous levels of protein in mammalian cells
  - PCK1 expression and purification from *E. coli*
  - PCK1 activity and kinetic assays
  - TIP60 acetylation assay
  - PCK1 expression and purification from HEK293T and pull-down assays
  - PCK1 expression and purification from mouse liver and kidney samples
  - PCK1 activity rescue and sirtuin *in vitro* deacetylation assays
  - Immunoprecipitation
  - GSK3β, SIRT1 and SIRT2 silencing
  - Cell fractionation
  - Glucose production assay
  - Glucose uptake experiments
  - $^{13}C_3$-pyruvate and $^{13}C_6$-glucose tracer experiments.
  - Kinase inhibition assays
  - Cycloheximide chase experiments
  - GSK3β assay
  - Peptide preparation and LC-MS/MS analysis
  - Molecular dynamics (MD) simulations in explicit solvent
- QUANTIFICATION AND STATISTICAL ANALYSIS
- DATA AND SOFTWARE AVAILABILITY

### SUPPLEMENTAL INFORMATION

Supplemental Information includes five figures, five tables, and four videos and can be found with this article online at https://doi.org/10.1016/j.molcel.2018.07.031.

## AUTHOR CONTRIBUTIONS

P.L.-M. and J.M.D. conceived of the project, designed and performed most experiments, interpreted data, and wrote the manuscript. J.B. designed and performed MS experiments and interpreted data. E.A.A. analyzed the metabolomics samples. R.H.-G. and F.C. designed and performed MD simulation experiments and interpreted data. L.E.W. and D.A.S. provided WT and SIRT1$^{-/-}$ mice tissue samples. P.L.-B. conceived of part of the project and revised the manuscript. J.A.C. conceived of, designed, and supervised PCK1 phosphorylation and ubiquitination experiments; interpreted data; and revised the manuscript.

## DECLARATION OF INTERESTS

D.A.S. is a consultant to Cohbar, EdenRoc Sciences, and Life Biosciences and their affiliates. J.M.D. is a consultant for BioTechne and FORGE Life Science and co-founder of Galilei BioSciences. The other authors declare no competing interests.

## REFERENCES

Arnold, K.M., Lee, S., and Denu, J.M. (2011). Processing mechanism and substrate selectivity of the core NuA4 histone acetyltransferase complex. Biochemistry 50, 727–737.

Baeza, J., Dowell, J.A., Smallegan, M.J., Fan, J., Amador-Noguez, D., Khan, Z., and Denu, J.M. (2014). Stoichiometry of site-specific lysine acetylation in an entire proteome. J. Biol. Chem. 289, 21326–21338.

Baeza, J., Smallegan, M.J., and Denu, J.M. (2015). Site-specific reactivity of nonenzymatic lysine acetylation. ACS Chem. Biol. 10, 122–128.

Beale, E.G., Hammer, R.E., Antoine, B., and Forest, C. (2004). Disregulated glyceroneogenesis: PCK1 as a candidate diabetes and obesity gene. Trends Endocrinol. Metab. 15, 129–135.

Beale, E.G., Harvey, B.J., and Forest, C. (2007). PCK1 and PCK2 as candidate diabetes and obesity genes. Cell Biochem. Biophys. 48, 89–95.

Beurel, E., Grieco, S.F., and Jope, R.S. (2015). Glycogen synthase kinase-3 (GSK3): regulation, actions, and diseases. Pharmacol. Ther. 148, 114–131.

Bian, Y., Song, C., Cheng, K., Dong, M., Wang, F., Huang, J., Sun, D., Wang, L., Ye, M., and Zou, H. (2014). An enzyme assisted RP-RPLC approach for in-depth analysis of human liver phosphoproteome. J. Proteomics 96, 253–262.

Borra, M.T., O'Neill, F.J., Jackson, M.D., Marshall, B., Verdin, E., Foltz, K.R., and Denu, J.M. (2002). Conserved enzymatic production and biological effect of O-acetyl-ADP-ribose by silent information regulator 2-like NAD+-dependent deacetylases. J. Biol. Chem. 277, 12632–12641.

Burgess, S.C., He, T., Yan, Z., Lindner, J., Sherry, A.D., Malloy, C.R., Browning, J.D., and Magnuson, M.A. (2007). Cytosolic phosphoenolpyruvate carboxykinase does not solely control the rate of hepatic gluconeogenesis in the intact mouse liver. Cell Metab. 5, 313–320.

Case, D.A., Darden, T.A., Cheatham, T.E., Simmerling, C.L., Wang, J., Duke, R.E., Luo, R., Walker, R.C., Zhang, W., Merz, K.M., et al. (2012). AMBER 12 (University of California, San Francisco, CA). http://ambermd.org/doc12/Amber12.pdf.

Caton, P.W., Nayuni, N.K., Khan, N.Q., Wood, E.G., and Corder, R. (2011). Fructose induces gluconeogenesis and lipogenesis through a SIRT1-dependent mechanism. J. Endocrinol. 208, 273–283.

Clasquin, M.F., Melamud, E., and Rabinowitz, J.D. (2012). LC-MS data processing with MAVEN: A metabolomic analysis and visualization engine. Curr. Protoc. Bioinformatics Chapter 14. Unit 14.11.

Cui, D.S., Broom, A., Mcleod, M.J., Meiering, E.M., and Holyoak, T. (2017). Asymmetric anchoring is required for efficient Ω-loop opening and closing in cytosolic phosphoenolpyruvate carboxykinase. Biochemistry 56, 2106–2115.

Darden, T., York, D., and Pedersen, L. (1993). Particle mesh Ewald: an N·log(N) method for Ewald sums in large systems. J. Chem. Phys. 98, 10089.

Demirkan, G., Yu, K., Boylan, J.M., Salomon, A.R., and Gruppuso, P.A. (2011). Phosphoproteomic profiling of in vivo signaling in liver by the mammalian target of rapamycin complex 1 (mTORC1). PLoS ONE 6, e21729.

Escós, M., Latorre, P., Hidalgo, J., Hurtado-Guerrero, R., Carrodeguas, J.A., and López-Buesa, P. (2016). Kinetic and functional properties of human mitochondrial phosphoenolpyruvate carboxykinase. Biochem. Biophys. Rep. 7, 124–129.

Fan, J., Baeza, J., and Denu, J.M. (2016). Investigating histone acetylation stoichiometry and turnover rate. Methods Enzymol. 574, 125–148.

Fuhrer, T., Fischer, E., and Sauer, U. (2005). Experimental identification and quantification of glucose metabolism in seven bacterial species. J. Bacteriol. 187, 1581–1590.

Granner, D., Andreone, T., Sasaki, K., and Beale, E. (1983). Inhibition of transcription of the phosphoenolpyruvate carboxykinase gene by insulin. Nature 305, 549–551.

Grimsrud, P.A., Carson, J.J., Hebert, A.S., Hubler, S.L., Niemi, N.M., Bailey, D.J., Jochem, A., Stapleton, D.S., Keller, M.P., Westphall, M.S., et al. (2012). A quantitative map of the liver mitochondrial phosphoproteome reveals post-translational control of ketogenesis. Cell Metab. 16, 672–683.

Hakimi, P., Yang, J., Casadesus, G., Massillon, D., Tolentino-Silva, F., Nye, C.K., Cabrera, M.E., Hagen, D.R., Utter, C.B., Baghdy, Y., et al. (2007). Overexpression of the cytosolic form of phosphoenolpyruvate carboxykinase (GTP) in skeletal muscle repatterns energy metabolism in the mouse. J. Biol. Chem. 282, 32844–32855.

Hallows, W.C., Lee, S., and Denu, J.M. (2006). Sirtuins deacetylate and activate mammalian acetyl-CoA synthetases. Proc. Natl. Acad. Sci. USA 103, 10230–10235.

Hanson, R.W., and Reshef, L. (1997). Regulation of phosphoenolpyruvate carboxykinase (GTP) gene expression. Annu. Rev. Biochem. 66, 581–611.

Hardie, D.G. (2004). AMP-activated protein kinase: a key system mediating metabolic responses to exercise. Med. Sci. Sports Exerc. 36, 28–34.

Herzig, S., and Shaw, R.J. (2018). AMPK: guardian of metabolism and mitochondrial homeostasis. Nat. Rev. Mol. Cell Biol. 19, 121–135.

Hirschey, M.D., Shimazu, T., Capra, J.A., Pollard, K.S., and Verdin, E. (2011). SIRT1 and SIRT3 deacetylate homologous substrates: AceCS1,2 and HMGCS1,2. Aging (Albany N.Y.) 3, 635–642.

Hod, Y., and Hanson, R.W. (1988). Cyclic AMP stabilizes the mRNA for phosphoenolpyruvate carboxykinase (GTP) against degradation. J. Biol. Chem. 263, 7747–7752.

Hopgood, M.F., Ballard, F.J., Reshef, L., and Hanson, R.W. (1973). Synthesis and degradation of phosphoenolpyruvate carboxylase in rat liver and adipose tissue 134, 445–453.

Horike, N., Sakoda, H., Kushiyama, A., Ono, H., Fujishiro, M., Kamata, H., Nishiyama, K., Uchijima, Y., Kurihara, Y., Kurihara, H., and Asano, T. (2008). AMP-activated protein kinase activation increases phosphorylation of glycogen synthase kinase 3β and thereby reduces cAMP-responsive element transcriptional activity and phosphoenolpyruvate carboxykinase C gene expression in the liver. J. Biol. Chem. 283, 33902–33910.

Jiang, W., Wang, S., Xiao, M., Lin, Y., Zhou, L., Lei, Q., Xiong, Y., Guan, K.L., and Zhao, S. (2011). Acetylation regulates gluconeogenesis by promoting PEPCK1 degradation via recruiting the UBR5 ubiquitin ligase. Mol. Cell 43, 33–44.

Jitrapakdee, S., Vidal-Puig, A., and Wallace, J.C. (2006). Anaplerotic roles of pyruvate carboxylase in mammalian tissues. Cell. Mol. Life Sci. 63, 843–854.

Johnson, T.A., and Holyoak, T. (2010). Increasing the conformational entropy of the Ω-loop lid domain in phosphoenolpyruvate carboxykinase impairs catalysis and decreases catalytic fidelity. Biochemistry 49, 5176–5187.

Johnson, T.A., and Holyoak, T. (2012). The Ω-loop lid domain of phosphoenolpyruvate carboxykinase is essential for catalytic function. Biochemistry 51, 9547–9559.

Johnson, T.A., Mcleod, M.J., and Holyoak, T. (2016). Utilization of substrate intrinsic binding energy for conformational change and catalytic function in phosphoenolpyruvate carboxykinase. Biochemistry 55, 575–587.

Khan, M.W., Biswas, D., Ghosh, M., Mandloi, S., Chakrabarti, S., and Chakrabarti, P. (2015). mTORC2 controls cancer cell survival by modulating gluconeogenesis. Cell Death Discov. 1, 15016.

Kim, E.Y., Kim, W.K., Kang, H.J., Kim, J.-H., Chung, S.J., Seo, Y.S., Park, S.G., Lee, S.C., and Bae, K.-H. (2012). Acetylation of malate dehydrogenase 1 promotes adipogenic differentiation via activating its enzymatic activity. J. Lipid Res. 53, 1864–1876.

Kiyohara, K., Gubbins, K.E., and Panagiotopoulos, A.Z. (1998). Phase coexistence properties of polarizable water models. Mol. Physiol. 94, 803–808.

Knyphausen, P., de Boor, S., Kuhlmann, N., Scislowski, L., Extra, A., Baldus, L., Schacherl, M., Baumann, U., Neundorf, I., and Lammers, M. (2016). Insights into lysine deacetylation of natively folded substrate proteins by sirtuins. J. Biol. Chem. 291, 14677–14694.

Kosanam, H., Thai, K., Zhang, Y., Advani, A., Connelly, K.A., Diamandis, E.P., and Gilbert, R.E. (2014). Diabetes induces lysine acetylation of intermediary metabolism enzymes in the kidney. Diabetes 63, 2432–2439.

Latorre, P., Burgos, C., Hidalgo, J., Varona, L., Carrodeguas, J.A., and López-Buesa, P. (2016). c.A2456C-substitution in Pck1 changes the enzyme kinetic and functional properties modifying fat distribution in pigs. Sci. Rep. 6, 19617.

Lin, Y.Y., Lu, J.Y., Zhang, J., Walter, W., Dang, W., Wan, J., Tao, S.C., Qian, J., Zhao, Y., Boeke, J.D., et al. (2009). Protein acetylation microarray reveals that NuA4 controls key metabolic target regulating gluconeogenesis. Cell 136, 1073–1084.

Lipina, C., Huang, X., Finlay, D., McManus, E.J., Alessi, D.R., and Sutherland, C. (2005). Analysis of hepatic gene transcription in mice expressing insulin-insensitive GSK3. Biochem. J. 392, 633–639.

Liu, X., Chhipa, R.R., Nakano, I., and Dasgupta, B. (2014). The AMPK inhibitor compound C is a potent AMPK-independent antiglioma agent. Mol. Cancer Ther. 13, 596–605.

Llanos, S., Cuadrado, A., and Serrano, M. (2009). MSK2 inhibits p53 activity in the absence of stress. Sci. Signal. 2, ra57.

Lundby, A., Lage, K., Weinert, B.T., Bekker-Jensen, D.B., Secher, A., Skovgaard, T., Kelstrup, C.D., Dmytriyev, A., Choudhary, C., Lundby, C., and Olsen, J.V. (2012). Proteomic analysis of lysine acetylation sites in rat tissues reveals organ specificity and subcellular patterns. Cell Rep. 2, 419–431.

Maier, J.A., Martinez, C., Kasavajhala, K., Wickstrom, L., Hauser, K.E., and Simmerling, C. (2015). ff14SB: improving the accuracy of protein side chain and backbone parameters from ff99SB. J. Chem. Theory Comput. 11, 3696–3713.

Montal, E.D., Dewi, R., Bhalla, K., Ou, L., Hwang, B.J., Ropell, A.E., Gordon, C., Liu, W.J., DeBerardinis, R.J., Sudderth, J., et al. (2015). PEPCK coordinates the regulation of central carbon metabolism to promote cancer cell growth. Mol. Cell 60, 571–583.

Owen, O.E., Kalhan, S.C., and Hanson, R.W. (2002). The key role of anaplerosis and cataplerosis for citric acid cycle function. J. Biol. Chem. 277, 30409–30412.

Papamokos, G.V., Tziatzos, G., Papageorgiou, D.G., Georgatos, S.D., Politou, A.S., and Kaxiras, E. (2012). Structural role of RKS motifs in chromatin interactions: a molecular dynamics study of HP1 bound to a variably modified histone tail. Biophys. J. 102, 1926–1933.

Parker, B.L., Yang, G., Humphrey, S.J., Chaudhuri, R., Ma, X., Peterman, S., and James, D.E. (2015). Targeted phosphoproteomics of insulin signaling using data-independent acquisition mass spectrometry. Sci. Signal. 8, rs6–rs6.

Pavlova, N.N., Hui, S., Ghergurovich, J.M., Fan, J., Intlekofer, A.M., White, R.M., Rabinowitz, J.D., Thompson, C.B., and Zhang, J. (2018). As extracellular glutamine levels decline, asparagine becomes an essential amino acid. Cell Metab. 27, 428–438.

Philippidis, H., Hanson, R.W., Reshef, L., Hopgood, M.F., and Ballard, F.J. (1972). The initial synthesis of proteins during development. Phosphoenolpyruvate carboxylase in rat liver at birth. Biochem J. 126, 1127–1134.

Price, N.L., Gomes, A.P., Ling, A.J.Y., Duarte, F.V., Martin-Montalvo, A., North, B.J., Agarwal, B., Ye, L., Ramadori, G., Teodoro, J.S., et al. (2012). SIRT1 is required for AMPK activation and the beneficial effects of resveratrol on mitochondrial function. Cell Metab. 15, 675–690.

Purushotham, A., Schug, T.T., Xu, Q., Surapureddi, S., Guo, X., and Li, X. (2009). Hepatocyte-specific deletion of SIRT1 alters fatty acid metabolism and results in hepatic steatosis and inflammation. Cell Metab. 9, 327–338.

Robles, M.S., Humphrey, S.J., and Mann, M. (2017). Phosphorylation is a central mechanism for circadian control of metabolism and physiology. Cell Metab. 25, 118–127.

Rodgers, J.T., and Puigserver, P. (2007). Fasting-dependent glucose and lipid metabolic response through hepatic sirtuin 1. Proc. Natl. Acad. Sci. USA 104, 12861–12866.

Rodgers, J.T., Lerin, C., Haas, W., Gygi, S.P., Spiegelman, B.M., and Puigserver, P. (2005). Nutrient control of glucose homeostasis through a complex of PGC-1alpha and SIRT1. Nature 434, 113–118.

Satapati, S., Sunny, N.E., Kucejova, B., Fu, X., He, T.T., Méndez-Lucas, A., Shelton, J.M., Perales, J.C., Browning, J.D., and Burgess, S.C. (2012). Elevated TCA cycle function in the pathology of diet-induced hepatic insulin resistance and fatty liver. J. Lipid Res. 53, 1080–1092.

Shao, J., Qiao, L., Janssen, R.C., Pagliassotti, M., and Friedman, J.E. (2005). Chronic hyperglycemia enhances PEPCK gene expression and hepatocellular glucose production via elevated liver activating protein/liver inhibitory protein ratio. Diabetes 54, 976–984.

She, P., Shiota, M., Shelton, K.D., Chalkley, R., Postic, C., and Magnuson, M.A. (2000). Phosphoenolpyruvate carboxykinase is necessary for the integration of hepatic energy metabolism. Mol. Cell. Biol. 20, 6508–6517.

She, P., Burgess, S.C., Shiota, M., Flakoll, P., Donahue, E.P., Malloy, C.R., Sherry, A.D., and Magnuson, M.A. (2003). Mechanisms by which liver-specific PEPCK knockout mice preserve euglycemia during starvation. Diabetes 52, 1649–1654.

Shen, Z., Wang, B., Luo, J., Jiang, K., Zhang, H., Mustonen, H., Puolakkainen, P., Zhu, J., Ye, Y., and Wang, S. (2016). Global-scale profiling of differential expressed lysine acetylated proteins in colorectal cancer tumors and paired liver metastases. J. Proteomics 142, 24–32.

Solovjeva, O.N., Kovina, M.V., and Kochetov, G.A. (2016). Substrate inhibition of transketolase. Biochim. Biophys. Acta 1864, 280–282.

Su, Z., Boersma, M.D., Lee, J.-H., Oliver, S.S., Liu, S., Garcia, B.A., and Denu, J.M. (2014). ChIP-less analysis of chromatin states. Epigenetics Chromatin 7, 7.

Sunny, N.E., Parks, E.J., Browning, J.D., and Burgess, S.C. (2011). Excessive hepatic mitochondrial TCA cycle and gluconeogenesis in humans with nonalcoholic fatty liver disease. Cell Metab. 14, 804–810.

Switzer, R.L., and Sogin, D.C. (1973). Regulation and mechanism of phosphoribosylpyrophosphate synthetase. V. Inhibition by end products and regulation by adenosine diphosphate. J. Biol. Chem. 248, 1063–1073.

Tilghman, S.M., Hanson, R.W., Reshef, L., Hopgood, M.F., and Ballard, F.J. (1974). Rapid loss of translatable messenger RNA of phosphoenolpyruvate carboxykinase during glucose repression in liver. Proc. Natl. Acad. Sci. USA 71, 1304–1308.

Wagner, S.A., Beli, P., Weinert, B.T., Schölz, C., Kelstrup, C.D., Young, C., Nielsen, M.L., Olsen, J.V., Brakebusch, C., and Choudhary, C. (2012). Proteomic analyses reveal divergent ubiquitylation site patterns in murine tissues. Mol. Cell. Proteomics 11, 1578–1585.

Wang, Q., Zhang, Y., Yang, C., Xiong, H., Lin, Y., Yao, J., Li, H., Xie, L., Zhao, W., Yao, Y., et al. (2010). Acetylation of metabolic enzymes coordinates carbon source utilization and metabolic flux. Science 327, 1004–1007.

Wang, R.H., Kim, H.S., Xiao, C., Xu, X., Gavrilova, O., and Deng, C.X. (2011). Hepatic Sirt1 deficiency in mice impairs mTorc2/Akt signaling and results in hyperglycemia, oxidative damage, and insulin resistance. J. Clin. Invest. 121, 4477–4490.

Weinert, B.T., Schölz, C., Wagner, S.A., Iesmantavicius, V., Su, D., Daniel, J.A., and Choudhary, C. (2013). Lysine succinylation is a frequently occurring

modification in prokaryotes and eukaryotes and extensively overlaps with acetylation. Cell Rep. *4*, 842–851.

Wilson-Grady, J.T., Haas, W., and Gygi, S.P. (2013). Quantitative comparison of the fasted and re-fed mouse liver phosphoproteomes using lower pH reductive dimethylation. Methods *61*, 277–286.

Xiao, Y., Nagai, Y., Deng, G., Ohtani, T., Zhu, Z., Zhou, Z., Zhang, H., Ji, M.Q., Lough, J.W., Samanta, A., et al. (2014). Dynamic interactions between TIP60 and p300 regulate FOXP3 function through a structural switch defined by a single lysine on TIP60. Cell Rep. *7*, 1471–1480.

Xu, H., Yang, Q., Shen, M., Huang, X., Dembski, M., Gimeno, R., Tartaglia, L.A., Kapeller, R., and Wu, Z. (2005). Dual specificity MAPK phosphatase 3 activates PEPCK gene transcription and increases gluconeogenesis in rat hepatoma cells. J. Biol. Chem. *280*, 36013–36018.

Yang, J., Kalhan, S.C., and Hanson, R.W. (2009a). What is the metabolic role of phosphoenolpyruvate carboxykinase? J. Biol. Chem. *284*, 27025–27029.

Yang, J., Reshef, L., Cassuto, H., Aleman, G., and Hanson, R.W. (2009b). Aspects of the control of phosphoenolpyruvate carboxykinase gene transcription. J. Biol. Chem. *284*, 27031–27035.

Yang, L., Vaitheesvaran, B., Hartil, K., Robinson, A.J., Hoopmann, M.R., Eng, J.K., Kurland, I.J., and Bruce, J.E. (2011). The fasted/fed mouse metabolic acetylome: N6-acetylation differences suggest acetylation coordinates organ-specific fuel switching. J. Proteome Res. *10*, 4134–4149.

Yang, H., Zhou, L., Shi, Q., Zhao, Y., Lin, H., Zhang, M., Zhao, S., Yang, Y., Ling, Z.-Q., Guan, K.-L., et al. (2015). SIRT3-dependent GOT2 acetylation status affects the malate-aspartate NADH shuttle activity and pancreatic tumor growth. EMBO J. *34*, 1110–1125.

Yu, W., Dittenhafer-Reed, K.E., and Denu, J.M. (2012). SIRT3 protein deacetylates isocitrate dehydrogenase 2 (IDH2) and regulates mitochondrial redox status. J. Biol. Chem. *287*, 14078–14086.

Yuan, Y., Hakimi, P., Kao, C., Kao, A., Liu, R., Janocha, A., Boyd-Tressler, A., Hang, X., Alhoraibi, H., Slater, E., et al. (2016). Reciprocal changes in phosphoenolpyruvate carboxykinase and pyruvate kinase with age are a determinant of aging in Caenorhabditis elegans. J. Biol. Chem. *291*, 1307–1319.

Zelle, R.M., Trueheart, J., Harrison, J.C., Pronk, J.T., and van Maris, A.J.A. (2010). Phosphoenolpyruvate carboxykinase as the sole anaplerotic enzyme in Saccharomyces cerevisiae. Appl. Environ. Microbiol. *76*, 5383–5389.

Zhao, S., Xu, W., Jiang, W., Yu, W., Lin, Y., Zhang, T., Yao, J., Zhou, L., Zeng, Y., Li, H., et al. (2010). Regulation of cellular metabolism by protein lysine acetylation. Science *327*, 1000–1004.

Zhou, B.P., Deng, J., Xia, W., Xu, J., Li, Y.M., Gunduz, M., and Hung, M.-C. (2004). Dual regulation of Snail by GSK-3β-mediated phosphorylation in control of epithelial-mesenchymal transition. Nat. Cell Biol. *6*, 931–940.

# STAR★METHODS

## KEY RESOURCES TABLE

| REAGENT or RESOURCE | SOURCE | IDENTIFIER |
| --- | --- | --- |
| Antibodies | | |
| Rabbit polyclonal DYKDDDDK (Flag) tag antibody | Cell Signaling Technology | Cat#2368; RRID: AB_2217020 |
| Mouse monoclonal tubulin antibody | Cell Signaling Technology | Cat#3873; RRID: AB_1904178 |
| Rabbit polyclonal SIRT1 antibody | Cell Signaling Technology | Cat#2310; RRID: AB_561272 |
| Rabbit monoclonal SIRT2 antibody | Cell Signaling Technology | Cat#12672; RRID: AB_2636961 |
| Rabbit multimonoclonal acetylated-lysine antibody | Cell Signaling Technology | Cat#9814S; RRID: AB_10548766 |
| Rabbit polyclonal PCK1 antibody | Santa Cruz Biotech | Cat#sc-74825; RRID: AB_2160024 |
| Rabbit monoclonal HA tag antibody | Cell Signaling Technology | Cat#3724; RRID: AB_1549585 |
| Rabbit polyclonal P300 antibody | Novus Biologicals | Cat#NB500-161; RRID: AB_350605 |
| Rabbit polyclonal phosphoserine/threonine antibody | Abcam | Cat#Ab17464; RRID: AB_443891 |
| Mouse monoclonal myc tag antibody | Thermo Fisher Scientific | Cat#MA1-980; RRID: AB_558470 |
| Mouse monoclonal ubiquitin antibody | Cell Signaling Technology | Cat#3936; RRID: AB_331292 |
| Rabbit polyclonal actin antibody | Sigma-Aldrich | Cat# A2066; RRID: AB_476693 |
| Rabbit polyclonal pyruvate carboxylase antibody | Thermo Fisher Scientific | Cat#PA5-50101; RRID: AB_2635554 |
| Bacterial and Virus Strains | | |
| *E. coli* BL21 DE3 cells | (Baeza et al., 2014) | N/A |
| *E. coli* BL21 DE3 ΔCobB cells | (Baeza et al., 2014) | N/A |
| *E. coli* Stellar cells | Clontech | Cat#636763 |
| Chemicals, Peptides, and Recombinant Proteins | | |
| IPTG | Gold Biotechnology | Cat# I2481C100 |
| HEPES | Fisher Scientific | Cat# BP310-1 |
| TCEP | Gold Biotechnology | Cat# TCEP25 |
| NP-40 | Sigma-Aldrich | Cat# NP40S |
| PreScission Protease | GE Healthcare | Cat# 27-0843-01 |
| N-ε-acetyl-lysine | Chem Impex International | Cat# 05364 |
| Oxaloacetic acid | Sigma-Aldrich | Cat# O4126 |
| GTP | Sigma-Aldrich | Cat# G8877 |
| Phosphoenolpyruvate | Bachem | Cat# Q-1640 |
| GDP | Sigma-Aldrich | Cat# G7127 |
| $KHCO_3$ | Fisher Scientific | Cat# P235-500 |
| NADH | Sigma-Aldrich | Cat# N4505 |
| $NAD^+$ | Sigma-Aldrich | Cat# N0632 |
| $MnCl_2$ | Fisher Scientific | Cat# BP214-500 |
| $MgCl_2$ | Fisher Scientific | Cat# AC223210025 |
| Dithiotreitol | Gold Biotechnology | Cat# DTT100 |
| Sucrose | Sigma-Aldrich | Cat# S0389 |
| Acetyl-CoA | Sigma-Aldrich | Cat# A2056 |
| Nicotinamide | Sigma-Aldrich | Cat# 72340 |
| NaF | Fisher Scientific | Cat# AC24325000 |
| Sodium pyrophosphate | Sigma-Aldrich | Cat# P8010 |
| Sodium orthovanadate | Sigma-Aldrich | Cat# S6508 |
| Dynabeads Protein G | Thermo Fisher Scientific | Cat# 10003D |
| Sodium Pyruvate | Sigma-Aldrich | Cat# P2256 |
| Sodium Lactate | Sigma-Aldrich | Cat# L7022 |

*(Continued on next page)*

*Continued*

| REAGENT or RESOURCE | SOURCE | IDENTIFIER |
| --- | --- | --- |
| PMSF | Gold Biotechnology | Cat# P470-10 |
| Aprotinin | Gold Biotechnology | Cat# A655-25 |
| Leupeptin | Gold Biotechnology | Cat#L-010-100 |
| Tween 20 | Sigma-Aldrich | Cat# P9416 |
| D6-acetic anhydride | Cambridge Isotopes | Cat# DLM-1162-PK |
| Trypsin | Thermo Fisher Scientific | Cat# 90058 |
| GluC | Thermo Fisher Scientific | Cat# 90054 |
| 3M Empore C18 47 mm extraction disks | Thermo Fisher Scientific | Cat# 14-386-2 |
| Waters Atlantis dC18 reverse phase column | Waters Atlantis | Cat# 186001317 |
| Lipofectamine RNAiMAX | Thermo Fisher Scientific | Cat# 13778030 |
| Genejuice | Novagen | Cat# 70967 |
| Ni-Sepharose 6 fast flow resin | GE Healthcare | Cat# 17-5318-01 |
| HiTrap Chelating HP 5 mL nickel column | GE Healthcare | Cat# 17-0408-01 |
| Superdex 26/60 200 pg GF column | GE Healthcare | Cat# 28-9893-36 |
| Aurum cation exchange columns | Bio Rad | Cat# 7326703 |
| Pierce Strong Anion exchange mini spin columns | Thermo Fisher Scientific | Cat# 90010 |
| Ammonium sulfate | Thermo Fisher Scientific | Cat# A701-50 |
| Bovine serum albumin | Sigma-Aldrich | Cat# A7906 |
| ProFection Mammalian transfection system | Promega | Cat# E1200 |
| Malic dehydrogenase | Sigma-Aldrich | Cat# M2634 |
| Pyruvate kinase-lactic dehydrogenase mix | Sigma-Aldrich | Cat# P0294 |
| Lactic dehydrogenase | Sigma-Aldrich | Cat# L2500 |
| Recombinant Histone H4 | (Su et al., 2014) | N/A |
| DMEM high (25 mM) glucose | Thermo Fisher Scientific | Cat# 11965 |
| DMEM no glucose | Thermo Fisher Scientific | Cat# A14430 |
| L-Glutamine | Thermo Fisher Scientific | Cat# 25030081 |
| Recombinant GSK3β | Abcam | Cat# Ab60863 |
| Dorsomorphin | Sigma-Aldrich | Cat# P5499 |
| CHIR99021 | Sigma-Aldrich | Cat# SLM1046 |
| SB 203580 | Sigma-Aldrich | Cat# S8307 |
| Rapamycin | Sigma-Aldrich | Cat# R0395 |
| MG132 | Sigma-Aldrich | Cat# M7449 |
| Cycloheximide | Sigma-Aldrich | Cat# C4859 |
| C646 (p300 inhibitor) | Sigma-Aldrich | Cat# 382113 |
| β-mercaptoethanol | Scharlau | Cat# ME00950250 |
| Tamoxifen citrate | Cayman Chemical | Cat# 54965-24-1 |
| U-$^{13}C_6$-Glucose | Cambridge Isotope Laboratories | Cat# CLM-1396 |
| U-$^{13}C_3$-Pyruvate | Cambridge Isotope Laboratories | Cat# CLM-1575 |
| Critical Commercial Assays | | |
| Glucose assay | Sigma-Aldrich | Cat# GAGO20 |
| Glucose Uptake-Glo Assay | Promega | Cat# J1341 |
| Q5 Site-Directed Mutagenesis kit | New England Biolabs | Cat# E0554S |
| Q5 high-fidelity DNA polymerase | New England Biolabs | Cat# E0555S |
| Deposited Data | | |
| Raw image files | This study, Mendeley Data | https://doi.org/10.17632/25kvr7zbzbk.1 |
| Experimental Models: Cell Lines | | |
| HEK293T | ATCC | Cat# CRL-3216 |
| HepG2 | ATCC | Cat# HB-8065 |

(*Continued on next page*)

| REAGENT or RESOURCE | SOURCE | IDENTIFIER |
|---|---|---|
| **Experimental Models: Organisms/Strains** | | |
| Tamoxifen Sirt1$^{-/-}$ inducible mice: C57BL6/AusbJ | (Price et al., 2012) | N/A |
| **Oligonucleotides** | | |
| Lysine to glutamine mutants | Table S5 | N/A |
| Lysine to acetyl-lysine mutants | Table S5 | N/A |
| SIRT1 and SIRT2 RNAi oligos | Table S5 | N/A |
| GSK3β SiRNA assay | Thermo Fisher Scientific | Cat#s6239 |
| Pyruvate carboxylase SiRNA assay | Thermo Fisher Scientific | Cat#s10089 |
| **Recombinant DNA** | | |
| Rat (*Rattus norvegicus*) Pck1 cDNA | GenScript | Cat# ORa12170 |
| Plasmid: pET22b-SUMO | (Escós et al., 2016) | N/A |
| Plasmid: pET22b-SUMO-Pck1 (rat) | This paper | N/A |
| Plasmid: pET22b-ULP1 | (Escós et al., 2016) | N/A |
| Plasmid: pCMV-HA | Clontech | Cat#631604 |
| Plasmid: pCMV-HA-Pck1-6xHis | This paper | N/A |
| Plasmid: pCDF-Duet1 | Novagen | Cat#TB390 |
| Plasmid: pCDF-Duet1-Pck1 | This paper | N/A |
| Plasmid: P300-HA | (Llanos et al., 2009) | N/A |
| Plasmid: Acetyl-lysine tRNA synthetase | (Yu et al., 2012) | N/A |
| Plasmid: Flag-SIRT1 | (Hirschey et al., 2011) | N/A |
| Plasmid: Flag-SIRT1 H363Y | (Hirschey et al., 2011) | N/A |
| Plasmid: TIP60 complex | (Arnold et al., 2011) | N/A |
| Plasmid: His tagged SIRT1 | (Hallows et al., 2006) | N/A |
| Plasmid: His tagged SIRT2 | (Borra et al., 2002) | N/A |
| Plasmid: GSK3β-myc | Addgene (Zhou et al., 2004) | Cat#16260 |
| **Software and Algorithms** | | |
| AMBER 12 with ff14SB force field | (Case et al., 2012; Maier et al., 2015) | N/A |
| GraphPad 6 | GrahPad software | N/A |
| Xcalibur | Thermo Fisher Scientific | N/A |
| ImageJ | NIH | N/A |

## CONTACT FOR REAGENT AND RESOURCE SHARING

Further information and requests for resources and reagents should be directed to and will be fulfilled by the Lead Contact, John M. Denu (john.denu@wisc.edu).

## EXPERIMENTAL MODEL AND SUBJECT DETAILS

### SIRT1$^{+/+}$ and SIRT1$^{-/-}$ mice

Tamoxifen inducible knockout mice as previously described (Price et al., 2012) were freshly backcrossed onto the C57BL6/AusbJ background. Mice were maintained on a 12 hr light cycle (0700/1900) in individually ventilated cages at 22 ± 1°C, 80% humidity at a density of 5 mice per cage. Animals were fed a standard chow diet from Gordon's Specialty Feeds (Yanderra, NSW Australia) comprising 8% calories from fat, 21% calories from protein, and 71% calories from carbohydrates, with a total energy density of 2.6 kcal/g. Males and females were bred as homozygotes for the SIRT1 stop allele, with males heterozygous for the ERT-Cre allele, and females wild-type for this allele. Offspring were born at the expected ratio, and all experimental comparisons were between male littermates. At 14 months of age, animals received chow diet containing tamoxifen citrate (360 mg/kg, Cayman Chemicals, formulated into chow diet AIN-93G by Dyets, PA USA) for 4 weeks to induce SIRT1 deletion. To reduce the impact of taste aversion to this diet, pellets were crushed, moistened with water, a small drop of almond essence added, and placed in the floor of cage. Diets were then reverted to standard chow without tamoxifen until 18 months of age, when animals were euthanized by cervical dislocation. Freshly dissected tissues were snap frozen, and later ground into powder using a mortar and pestle sitting in dry ice. These

experiments were performed under UNSW animal care and ethics committee (ACEC) number 13/134B, complying with the Australian Code for the Care and Use of Animals for Scientific Purposes, 8th Edition 2013.

### Cell cultures

HEK293T cells were maintained in DMEM supplemented with 10% FBS. Cells were transfected using either ProFection Mammalian Transfection System (Promega), Lipofectamine RNAiMAX (Thermo Fisher Scientific) or Genejuice (Novagen), as specified.

HepG2 cells were maintained in MEM supplemented with 10% FBS. RNAi and plasmid reverse transfections were performed using Lipofectamine RNAiMAX (Thermo Fisher Scientific) and Genejuice (Novagen), respectively.

For the experiments using 6-well plates the amount of each plasmid used per well was 1 $\mu$g. Unless specified, this amount of DNA was scaled up or down according to the plate used for each experiment.

Both RNAi and plasmid constructs transfection reactions were performed separately. Cells were harvested 48 hours post-transfection.

No-glucose DMEM was supplemented with 4 mM L-glutamine (Thermo Fisher Scientific), the same concentration present in high glucose DMEM. High and no-glucose DMEM were mixed to obtain the desired concentration of glucose. Then, media were added to each well and cells were harvested 24 hours later. When specified, media were supplemented with 10% FBS.

## METHOD DETAILS

### Determination of endogenous levels of protein in mammalian cells

HEK293T cells ($5 \times 10^5$) were grown on 6-well plates in DMEM supplemented with 10% FBS at 37°C, 5% $CO_2$ and humidified atmosphere. HepG2 cells ($1 \times 10^6$) were grown in MEM supplemented with 10% FBS. 24 h after seeding, media were replaced with fresh one containing different glucose concentrations: 2.5, 5, 10, 15, 20 and 25 mM, with or without FBS as specified. Media were prepared by mixing DMEM containing 25 mM (4.5 g/L) glucose with glucose-free DMEM to reach the desired glucose concentration. After 24 h cells were harvested and lysed in cold PBS supplemented with 1% NP40, PMSF, leupeptin and aprotinin. Lysates were incubated on ice for 15 minutes. Then, they were vortexed and after a freeze-thaw cycle they were centrifuged at 14000 $g$ for 10 minutes. Supernatant was collected and protein levels analyzed by WB. In the case of HepG2 cells, this experiment was exactly repeated but confluency was reached 48 hours after seeding. These experiments were repeated at least twice. Protein levels were measured by band densitometry using ImageJ (NIH) and normalized to the tubulin content.

### PCK1 expression and purification from *E. coli*

For the generation of K to Q and K to AcK mutants see oligos in Table S5. *E. coli* BL21 DE3 were grown in 2xYT supplemented with ampicillin (200 $\mu$g/mL) until OD600 reached 0.4. Cells were cooled down to 25°C and induced using 1 mM IPTG at 18°C overnight. Pellet was collected by centrifugation at 8000 $g$ and resuspended in PCK1 buffer A (25 mM HEPES, pH 7.5, 1 mM TCEP, 10 mM imidazole and 500 mM NaCl) supplemented with 1% NP-40, lysozyme, aprotinin, leupeptin, PMSF and DNase I. Cells were lysed using a Sonic Dismembrator sonicator (Thermo Fisher Scientific) (100W, 30 s on/30 s off and a 5-minute sonication). Lysate was centrifuged at 40,000 $g$ for 15 minutes and 4°C. Supernatant was filtered through a 0.45 $\mu$m filter. Protein mixture was loaded into a 5 mL HiTrap Chelating HP nickel column (GE Healthcare) pre-equilibrated in PCK1 buffer A. PCK1 was eluted using PCK1 buffer B (25 mM HEPES, pH 7.5, 150 mM NaCl, 1 mM TCEP and 500 mM imidazole). Protein purity was analyzed by SDS-PAGE, concentrated and desalted using an Amicon 30 kDa filter (Millipore) in PCK1 buffer C (25 mM HEPES, pH 7.5, 150 mM NaCl and 1 mM TCEP). Protein cleavage was performed using ULP1 (1:100 ratio mg/mg) at 4°C overnight. After protein cleavage, PCK1 was loaded into a nickel column equilibrated in buffer C and collected in the flow-through. Protein was concentrated, quantified by $Abs_{280}$ ($\varepsilon = 1.568$ mL/mg), aliquoted, flash-frozen in liquid nitrogen and stored at $-80$°C.

Lysine to acetyl-lysine variants were purified as described above with the following modifications. *E. coli* BL21 $\Delta$CobB strain, containing both the desired PCK1 mutant and the AcK-RS (acetyl-lysine tRNA Synthetase), was used. When $OD_{600}$ reached 0.4, N-$\varepsilon$-acetyl-lysine (Chem-Impex International) was added to a final concentration of 10 mM. Cells were incubated at room temperature for 30 minutes and induced using 0.5 mM IPTG at 18°C overnight. A cobalt column was used for purification. PCK1 eluted from the cobalt column was concentrated in a 30 kDa Amicon, diluted in buffer C and the His tag removed using PreScission Protease (1:100 mg/mg) overnight at 4°C. Finally, PCK1 was dialyzed against PCK1 buffer C, then concentrated, aliquoted and stored at $-80$°C.

### PCK1 activity and kinetic assays

Oxaloacetic acid (OAA), GTP, GDP, ADP and NADH were from Sigma. Phosphoenolpyruvate (PEP) was from Bachem. Dithiothreitol (DTT) was from Gold Biotechnology. Enzymes, malic dehydrogenase (MDH, M2634), pyruvate kinase/Lactic dehydrogenase (PK/LDH, P0294) mix and lactic dehydrogenase (LDH, L2500) were from Sigma. PCK1 activity was measured in 96-well plates in a total volume of 100 $\mu$L at 30°C using a Synergy H4 plate reader (Biotek) recording NADH oxidation in continuous mode. Coupled assays were used as previously described (Johnson and Holyoak, 2012; Latorre et al., 2016). Each assay in the OAA to PEP reaction consisted of 100 mM HEPES, pH 7.5, 0.4 mM OAA, 1 mM GTP, 1 mM ADP, 0.4 mM NADH, 4 mM MgCl2, 0.2 mM MnCl2, 10 mM DTT, 0.5 units of PK/LDH and 14 nM PCK1. Reaction was started by the addition of OAA. In the PEP to OAA reaction, each well contained

100 mM HEPES, pH 7.5, 100 mM KHCO$_3$, 2 mM PEP, 2 mM GDP, 0.4 mM NADH, 10 mM DTT, 8 mM MgCl2, 0.2 mM MnCl2, 0.4 units of MDH and 28 nM PCK1. Reaction was started by the addition of PCK1. Each substrate concentration was accordingly varied to determine kinetic constants. The pyruvate kinase assay was performed as the OAA to PEP reaction but excluding PK/LDH mix and ADP from the reaction and including 0.8 units of LDH. PCK1 WT and K-AcK mutants were used at a concentration of 350 and 140 nM, respectively. Enolate retention assays (also half-reaction) were performed as described (Johnson and Holyoak, 2012), the phosphoryl donor GTP was replaced with GDP. PCK1 concentration was 140 nM for this assay. For every experiment, PCK1 was prepared as a 10x solution in fresh 25 mM HEPES, pH 7.5, 10 mM DTT.

### TIP60 acetylation assay

Recombinant PCK1 (7 μM) or histone H4 (7 μM) were independently incubated in the presence of TIP60 complex (1 μM). Acetylation buffer consisted of 50 mM Tris-HCl, pH 8, 150 mM NaCl, 10% glycerol, 1 mM DTT, 0.5 mM PMSF and 0.2 mM EDTA. Acetyl CoA was added to a final concentration of 1 mM. Reactions took place at 30°C for 1 hour or overnight in a total volume of 50μL. Only substrates (PCK1 or H4) or substrates in the presence of acetyl-CoA or substrates with only TIP60 were used as controls.

### PCK1 expression and purification from HEK293T and pull-down assays

HEK293T cells were grown in DMEM supplemented with 10% FBS on 150 mm plates. When cells were confluent, one third of the cells in the plate were seeded on new 150 mm plates with fresh media. Cells were incubated overnight as described. Cells were transfected using Profection Mammalian Transfection System (Promega) following manufacturer's instructions. 15 μg of each HA-PCK1-6xHis and P300-HA plasmids were used. 24 hours after transfection, media were replaced with fresh media containing 2.5, 5, 10, 15, 20 or 25 mM glucose without FBS and, when specified, cells were also treated with the p300 inhibitor C646 at a final concentration of 10 μM. After 24 hours, cells were harvested in pre-chilled PBS and centrifuged at 500 g and 4°C. Supernatant was removed and cells were resuspended in 0.8 mL of PCK1 buffer A supplemented with 1 mM nicotinamide (NAM), 1 mM sodium butyrate and protease inhibitors (aprotinin, leupeptin and PMSF). TCEP was replaced with 1 mM β-mercaptoethanol. 5 mM NaF, 5 mM sodium pyrophosphate and 1 mM sodium orthovanadate were added to resuspension buffer in the experiments analyzing PCK1 phosphorylation. Then, cells were lysed on ice in a 1 mL dounce homogenizer performing 40 strokes, using a tight pestle. Lysates were centrifuged at 14,000 g and 4°C, and supernatant was added to 0.5 mL of nickel-Sepharose resin (GE Healthcare) equilibrated in buffer A. After a 2h incubation at 4°C under rotation, nickel resin was pulled down at 500 g and 4°C and supernatant discarded. 1 mL of fresh buffer A was added and incubated under rotation for 5 minutes; this step was repeated three additional times. Next, resin was washed with 1 mL of PCK1 buffer A containing 50 mM imidazole for 10 minutes, to remove contaminants. This step was repeated twice. After that, two washes each containing 250 and 500 mM imidazole were performed to elute PCK1. Eluted protein purity was analyzed by SDS-PAGE and the protein was washed three times in a centrifugal filter using PCK1 buffer C and concentrated.

For pull-down assays, cells were grown on 6-well plates and harvested in PBS supplemented with deacetylase and phosphatase inhibitors. Pellets were flash-frozen in liquid nitrogen and resuspended in buffer A. PCK1 was pulled down using 50 μL of Ni-Sepharose resin under the conditions described above. Co-purification of PCK1 and GSK3β was performed as described but using 25 mM HEPES, pH 7.5, 150 mM NaCl, 10 mM imidazole, and 1 mM β-mercaptoethanol as buffer.

### PCK1 expression and purification from mouse liver and kidney samples

All purification steps were performed at 4°C. The presence of PCK1 was determined by checking its activity throughout the purification. Pulverized tissue samples from three different animals each group (WT and SIRT1$^{-/-}$) were resuspended in 5 mL of 25 mM HEPES, pH 7.5, 250 mM sucrose, 10 mM DTT, 2 mM NAM, 1 mM NaF and 1 mM PMSF and centrifuged at 50,000 g and 4°C for 45 minutes. Ammonium sulfate was added to supernatants to a final saturation of 45%. After 1 hour under incubation at 4°C, samples were centrifuged at 5,000 g for 15 minutes. PCK1 was collected in the supernatant. This process was repeated but, with addition of ammonium sulfate to a final saturation of 70%. PCK1 was collected in the pellet, resuspended in 25 mM HEPES, pH 7.5, 10 mM DTT, 2 mM NAM, 1 mM NaF and 1 mM PMSF and desalted in the same buffer using an Amicon 30 kDa filter. Samples were loaded into Aurum Cation Exchange columns (Bio-Rad) equilibrated in the same buffer. PCK1 was then collected in the flow through. PCK1 was loaded into a Pierce Strong Anion Exchange Mini Spin Column (Thermo Fisher Scientific) and eluted between 200 and 400 mM NaCl. Highest purity fractions were pooled and concentrated. Purity was checked by SDS-PAGE.

### PCK1 activity rescue and sirtuin *in vitro* deacetylation assays

PCK1 (1.4 μM) purified from HEK293T cells was incubated in the presence of either recombinant SIRT1 (0.35 μM) or SIRT2 (0.35 μM) in 20 mM sodium phosphate buffer, pH 7.5 supplemented with 0.5 mM NAD$^+$. Total volume was 20 μL. After 30 minutes at 30°C, PCK1 was diluted 10-fold in 25 mM HEPES, pH 7.5, 10 mM DTT and kept on ice. PCK1 activity was measured in both reaction directions as explained above. Controls included either PCK1 in the presence of 0.5 mM NAD$^+$ or PCK1 in the only presence of sirtuin. Deacetylation of 1 μg of recombinant PCK1 S90E+K91AcK mutant was performed in the presence of 0.5 mM NAD$^+$ for 2h or overnight. Deacetylation of recombinant acetylated K91AcK mutant was performed at 30°C for two hours in the presence of 2 mM NAD$^+$. 1 μg or 2 μg of PCK1 were used for western blotting or mass spectrometry assays, respectively.

## Immunoprecipitation

HEK293T cells ($7.5 \times 10^5$) were seeded on 6-well plates and incubated overnight. Cells were transfected as described. 2 μg of each HA-PCK1-6xHis, FLAG-SIRT1 and FLAG-SIRT1 H363Y construct were used. After 24 hours, media were replaced with fresh DMEM without FBS. 24 hours later, cells were washed twice in PBS containing 1 mM NAM, harvested, centrifuged at 500 g and 4°C, and lysed in PBS, 1% NP-40, 1 mM PMSF and 1 mM NAM on ice. After 15 minutes, samples were flash-frozen in liquid nitrogen and thawed. Lysates were centrifuged at 10000 g and 4°C and supernatant was incubated overnight with 4 μg of anti HA antibody at 4°C. Protein G Dynabeads (Invitrogen) were added to the tubes and incubated for 2 h at 4°C. After three 10-minute washes in PBS, SDS-PAGE sample buffer was added and samples were run in 10% acrylamide gels, protein transferred and membranes probed.

## GSK3β, SIRT1 and SIRT2 silencing

HEK293T ($7.5 \times 10^5$) and HepG2 ($1 \times 10^6$) cells were reverse transfected with the appropriate RNAi oligos (see Key Resources Table). Final concentration was 50 nM. Cells were grown on 6-well plates. GSK3β silencing was performed using siRNA. When specified, cells were also reverse transfected with pCMV-HA-PCK1-6xHis using GeneJuice (Novagen). This reaction was performed in a separate tube and mixed with the cells when plating. After 48 hours, cells were harvested and lysed as described.

## Cell fractionation

HepG2 and HEK293T cells were grown under different glucose concentrations. Cells were harvested and lysed in 20 mM HEPES, pH 7.5, 250 mM sucrose, 10 mM KCl, 2 mM $MgCl_2$, 1 mM EDTA and protease inhibitors using a 22G needle. Lysates were incubated for 20 minutes on ice and centrifuged at 700 g for 5 minutes. Supernatant containing mitochondria and cytosol was centrifuged again at 10000 *g* and supernatant containing cytosolic fraction was used to measure PCK1 activity as described. Activity was normalized to the PCK1 content determined by western blot.

## Glucose production assay

HEK293T cells ($3 \times 10^5$) were seeded on 12-well plates. Cells were transfected as described. After 24 hours, cells were carefully washed twice with PBS. 1 mL of glucose production medium was added to each well (DMEM without glucose and phenol red supplemented with 2 mM sodium pyruvate and 20 mM sodium lactate). Halves of the medium were collected at different time points and glucose was determined using a colorimetric kit (Sigma GAGO20). Glucose readings were normalized to the protein content from the whole cell lysates.

## Glucose uptake experiments

HEK293T cells ($5 \times 10^4$) were reverse transfected using either PCK1 WT or S90A constructs (62.5 ng/well) and seeded on 96-well plates. 48 hours after transfection glucose uptake was determined using Glucose Uptake-Glo assay (Promega) following manufacturer's instructions. Luminescence was recorded using a CLARIOstar luminometer (BMG Labtech) and normalized to the total protein content. PCK1 WT and S90A expression were also checked by western blotting.

## $^{13}C_3$-pyruvate and $^{13}C_6$-glucose tracer experiments.

HEK293T cells ($2.5 \times 10^6$) were reverse transfected using the PCK1 WT construct (3 μg) and and/or pyruvate carboxylase (PC) silencing oligos (final concentration of 50 nM in media), as specified in the main text. Cells were grown in DMEM on 100 mm plates. Media were renewed every 24 hours. Four days after transfection, media were replaced with DMEM containing either 25 mM $^{13}C_6$-glucose or 1 mM $^{13}C_3$-pyruvate. After 4 hours, media were removed and cells were quickly washed with PBS three times. Metabolites were extracted using 80% methanol and dried down. Samples were reconstituted to a concentration of 1 mg/ 200 μL using a buffer mix equivalent to the starting gradient condition, given one more hard spin to remove any remaining insoluble material, and supernatants were transferred to vials for LC-MS analysis. The LC-MS method involved reversed-phase ion-pairing chromatography on a Vanquish UHPLC coupled with negative mode ESI electrospray ionization and detection on a Q Exactive orbitrap mass spectrometer (Thermo Fisher Scientific). LC separation was performed with a Waters Acquity UPLC BEH C18 column (1.7 μm, 2.1 × 100 mm; Waters Corp.) over a 25' method with a 14.5′ gradient, ramping methanol from 5% to 95% against a buffer of water with 3% methanol, 10 mM tributyamine, and acetic acid-adjusted pH of 8.3. Injection volume was 10 μL, flow rate 200 μL/min, and column temperature 25°C. ESI settings were 30/ 10/ 1 sheath/ aux sweep gas rates, 2.50 |kV| spray voltage, S-lense RF level 50, 350°C capillary, and 300°C aux gas. MS1 scans were performed over a scan range of 85-1250 m/z at 70,000 resolution, AGC target of 1e6, and 100 ms maximum IT. Data were analyzed using MAVEN/ El-MAVEN (Clasquin et al., 2012; Pavlova et al., 2018) and Elucidata (http://www.elucidata.io/) and utilizing compound lists with retention times empirically determined in-house or by colleagues. Metabolite expression was captured using the AreaTop metric; exported data were analyzed in Excel (Microsoft).

## Kinase inhibition assays

HEK293T cells ($7.5 \times 10^5$) were grown on 6-well plates and reverse transfected as described. 24 hours after transfection, media were replaced with fresh DMEM supplemented with one of the following kinase inhibitors: 5 μM dorsomorphin (AMPK inhibitor), 5 μM CHIR99021 (GSK3 inhibitor), 5 μM SB 203580 (MAPK inhibitor) or 20 nM rapamycin (mTOR inhibitor). When specified, proteasome

inhibitor MG132 treatment was performed at 10 μM. Cells were exposed to each one of this compounds for 18 hours more. Cells were lysed and PCK1 was pulled down as described above.

### Cycloheximide chase experiments

HEK293T cells ($2 \times 10^5$) were grown on 24-well plates and reverse transfected using 20 ng of PCK1 or PCK1 S90A mutant constructs. After 24 hours media were replaced with DMEM supplemented with 100 μg/mL cycloheximide and cells were harvested at different time points: 0, 2, 4 and 8 hours. The presence of PCK1 was analyzed by western blotting and normalized to the actin content.

### GSK3β assay

Recombinant PCK1 (1.4 μM) was incubated at 37°C in the presence of recombinant GSK3β (0.35 μM) in 25 mM HEPES, pH 7.5, 10 mM DTT, 2 mM ATP and 10 mM $MgCl_2$ for 2 hours. Protein phosphorylation was analyzed by western blotting.

### Peptide preparation and LC-MS/MS analysis

The stoichiometry of pulled down PCK1 from HEK293T cells was determined as described previously with slight modification (Baeza et al., 2014). Briefly, 2 μg of PCK1 sample was resuspended into 25 μL of urea buffer (200 mM ammonium bicarbonate buffer pH = 8.0, 6 M deionized and filtered urea, 5 mM DTT). Each sample was heat denatured and reduced at 60°C for 20 minutes on Thermomixer at 1000 RPM. Cysteine alkylation was performed by adding 80 mM iodoacetamide to each sample and incubating at 37°C for 20 minutes on Thermomixer at 1000 RPM. The unmodified lysines were chemically acetylated by adding ~50 μmol of D6-acetic anhydride (99.8% isotopic purity, Cambridge Isotopes) and incubating 60°C for 20 minutes. Addition of acetic anhydride to the sample drops the pH of the solution, therefore ammonium hydroxide was used to raise the pH to ~8.5 followed by another round of chemical acetylation using D6-acetic anhydride. To hydrolyze any O-acetyl esters that may have formed during the chemical acetylation, the pH of the solution was raised to ~8.5 and incubated at 60°C for 20 minutes on the Thermomixer at 1000 RPM. The concentration of urea was diluted to 2 M by adding up to 75 μL final volume using 100 mM ammonium bicarbonate pH = 8.5. The samples were digested by adding 1 μg of trypsin and incubating for 4 hours at 37°C. To increase the peptide coverage, a second proteolytic step was conducted using GluC. For this step, the urea concentration was diluted to 1 M by adding up to 150 μL of 100 mM ammonium bicarbonate pH = 8.5 and adding 0.5 μg of GluC. The sample was digested overnight at 37°C on the Thermomixer at 500 RPM. Trypsin and GluC digested peptide samples were desalted prior to MS analysis as described previously (Fan et al., 2016). Desalting tips were prepared using 3M Empore C18 47mm extraction disks (model 2215). Peptides were separated with a Dionex Ultimate 3000 RSLC nano HPLC using a Waters Atlantis dC18 (100 μm × 150 mm) reverse phase column. Mobile phase consisted of 0.1% formic acid (A) and acetonitrile with 0.1% formic acid (B). Peptides were eluted with a linear gradient of 2%–40% B at a flow rate of 0.8 μl/min over 40 min and introduced into a hybrid quadrupole-Orbitrap mass spectrometer (Thermo Q Exactive) by nanoelectrospray ionization (Thermo Nanospray Flex). The MS survey scan was performed in positive ion mode with a resolution of 140,000, AGC of 3E6, maximum fill time of 100 ms, and scan range of 300 to 1200 m/z. Data-dependent MS/MS was performed with a resolution of 35,000, AGC of 2E5, maximum fill time of 100 ms, isolation window of 1.5 m/z, underfill ratio of 1.0%, a stepped collision energy of 25, 30, 35, dynamic exclusion of 10 s, and a loop count of 10. The source voltage was set at 2.3 kV and capillary temperature at 250°C. Protein and peptide identification was performed using a Mascot database. Trypsin and GluC were selected as enzymes. Cysteine alkylation was set as fixed modification and methionine oxidation, lysine acetylation and lysine acetylation (D3) were set as variable modifications. MS1 precursor tolerance was set to ± 10 ppm, and MS2 fragment mass tolerance was set to ± 0.01 Da. Peptide identifications were obtained using a false discovery rate of 1%. Acetylation stoichiometry for PCK1 peptides were determined as previously described (Baeza et al., 2015).

### Molecular dynamics (MD) simulations in explicit solvent

The simulations were carried out with AMBER 12 package (Case et al., 2012) with ff14SB (Maier et al., 2015). The crystal structure of rat cytosolic PCK1 in complex with oxalate and GTP (PDB: 3dt2) was used as starting coordinates in all the simulations. The structure was conveniently modified to contain the Lys91ac. The complex was then immersed in a water box with a 10 Å buffer of TIP3P water molecules (Kiyohara et al., 1998). A two-stage geometry optimization approach was performed. The first stage minimizes only the positions of solvent molecules and the second stage is an unrestrained minimization of all the atoms in the simulation cell. The systems were then gently heated by incrementing the temperature from 0 to 300 K under a constant pressure of 1 atm and periodic boundary conditions. Harmonic restraints of 30 kcal·mol-1 were applied to the solute, and the Andersen temperature-coupling scheme was used to control and equalize the temperature. The time step was kept at 1 fs during the heating stages, allowing potential inhomogeneities to self-adjust. Long-range electrostatic effects were modeled using the particle-mesh-Ewald method (Darden et al., 1993). An 8-Å cut-off was applied to Lennard-Jones and electrostatic interactions. Each system was equilibrated for 2 ns with a 2-fs time step at a constant volume and temperature of 300 K. Production trajectories were then run for additional 1.5 μs under the same simulation conditions. Simulations were carried out with and without ligands. The parameter reported for the acetylated lysine was employed in the simulations (Papamokos et al., 2012).

## QUANTIFICATION AND STATISTICAL ANALYSIS

When specified, WB band densitometry analysis was performed using ImageJ (NIH). MS data were analyzed using Xcalibur Software. Kinetic parameters were obtained by fitting data to the Michaelis-Menten equation using GraphPad Prism 6. For statistical analysis data normality was checked by performing Shapiro-Wilk tests. Then, two sample t tests were performed to compare means between groups. For metabolomics experiments, One-Way ANOVA tests were performed to check differences following Tukey HSD post hoc tests to determine differences between treatments. When $p < 0.05$, differences were considered significant; n represented the number of independent experiments; mean ± SD were represented.

## DATA AND SOFTWARE AVAILABILITY

Raw image files are deposited on Mendeley Data (https://doi.org/10.17632/25kvr7zbzk.1).